Structure and Dynamics of a Processive Brownian Motor: The Translating Ribosome

Joachim Frank[1,2] and Ruben L. Gonzalez, Jr.[3]

[1]Howard Hughes Medical Institute, Department of Biochemistry and Molecular Biophysics, Columbia University, New York City, New York 10032

[2]Department of Biological Sciences and [3]Department of Chemistry, Columbia University, New York City, New York 10027; email: jf2192@columbia.edu, rlg2118@columbia.edu

Annu. Rev. Biochem. 2010. 79:381–412

First published online as a Review in Advance on March 17, 2010

The *Annual Review of Biochemistry* is online at biochem.annualreviews.org

This article's doi: 10.1146/annurev-biochem-060408-173330

0066-4154/10/0707-0381$20.00

Key Words

cryo-EM, FRET, protein synthesis, ribosome, X-ray

Abstract

There is mounting evidence indicating that protein synthesis is driven and regulated by mechanisms that direct stochastic, large-scale conformational fluctuations of the translational apparatus. This mechanistic paradigm implies that a free-energy landscape governs the conformational states that are accessible to and sampled by the translating ribosome. This scenario presents interdependent opportunities and challenges for structural and dynamic studies of protein synthesis. Indeed, the synergism between cryogenic electron microscopic and X-ray crystallographic structural studies, on the one hand, and single-molecule fluorescence resonance energy transfer (smFRET) dynamic studies, on the other, is emerging as a powerful means for investigating the complex free-energy landscape of the translating ribosome and uncovering the mechanisms that direct the stochastic conformational fluctuations of the translational machinery. In this review, we highlight the principal insights obtained from cryogenic electron microscopic, X-ray crystallographic, and smFRET studies of the elongation stage of protein synthesis and outline the emerging themes, questions, and challenges that lie ahead in mechanistic studies of translation.

Contents

Translation: the process through which the ribosome synthesizes a protein by repeatedly incorporating aminoacyl-tRNAs as dictated by the messenger RNA

Cryogenic electron microscopy (cryo-EM): a technique for three-dimensional imaging of macromolecules in their native state with a transmission electron microscope

1. INTRODUCTION

Protein synthesis, or translation, is universally catalyzed by the ribosome, a massive, two-subunit ribonucleoprotein molecular machine (**Figure 1*a***). New insights into the relationship between the conformational dynamics of the ribosome, its transfer RNA (tRNA) substrates, and its translation cofactors, as well as the mechanical, catalytic, and regulatory events that drive protein synthesis, are altering our mechanistic understanding of translation. This is particularly true for the translation elongation cycle (**Figure 1*b***), where a wealth of biochemical, structural, dynamic, and computational data have begun to advance the view of the elongating ribosome as a processive stochastic molecular machine (1–4). Synthesis of the data, toward an understanding of the role of conformational dynamics, benefits from concepts developed in recent years in studies of biomolecular motors (5–7).

1.1. Principles Underlying the Operation of Biomolecular Motors

Biomolecular motors harness the energy released from a chemical reaction, typically hydrolysis of a so-called high-energy phosphate compound, such as ATP or GTP, to perform mechanical work. The detailed mechanisms through which these systems transduce the energy of ATP or GTP hydrolysis into mechanical work remains an area of intense research. Static structures of biomolecular motors, such as those furnished by cryogenic electron microscopy (cryo-EM) or X-ray crystallography, often evoke the impression of smoothly running, deterministic machines, much like their macroscopic counterparts, captured in "snapshots" at certain time points along their respective reaction coordinates. In reality, however, nanometer-scale biomolecular motors operate in an environment where they are constantly subjected to the stochastic Brownian forces that arise from collisions of the surrounding media with the motor and its parts and where viscous drag easily dominates inertia—conditions that prohibit the smooth, deterministic motion usually associated with macroscopic machines. Thus, it has been proposed that many biomolecular motors employ, or at least partially employ, Brownian motor mechanisms of operation (5–7).

The principal idea underlying a Brownian motor mechanism is that force or motion is drawn from the stochastic thermal fluctuations to which these systems are constantly subjected. Because random thermal noise itself cannot confer processivity to a biomolecular motor, the directedness of the process is typically imparted by "biasing" or "rectifying" the stochastically fluctuating system through the intervention of (*a*) a substrate, cofactor, or allosteric effector binding event; (*b*) an irreversible chemical step; or (*c*) the release or diffusion of a reaction

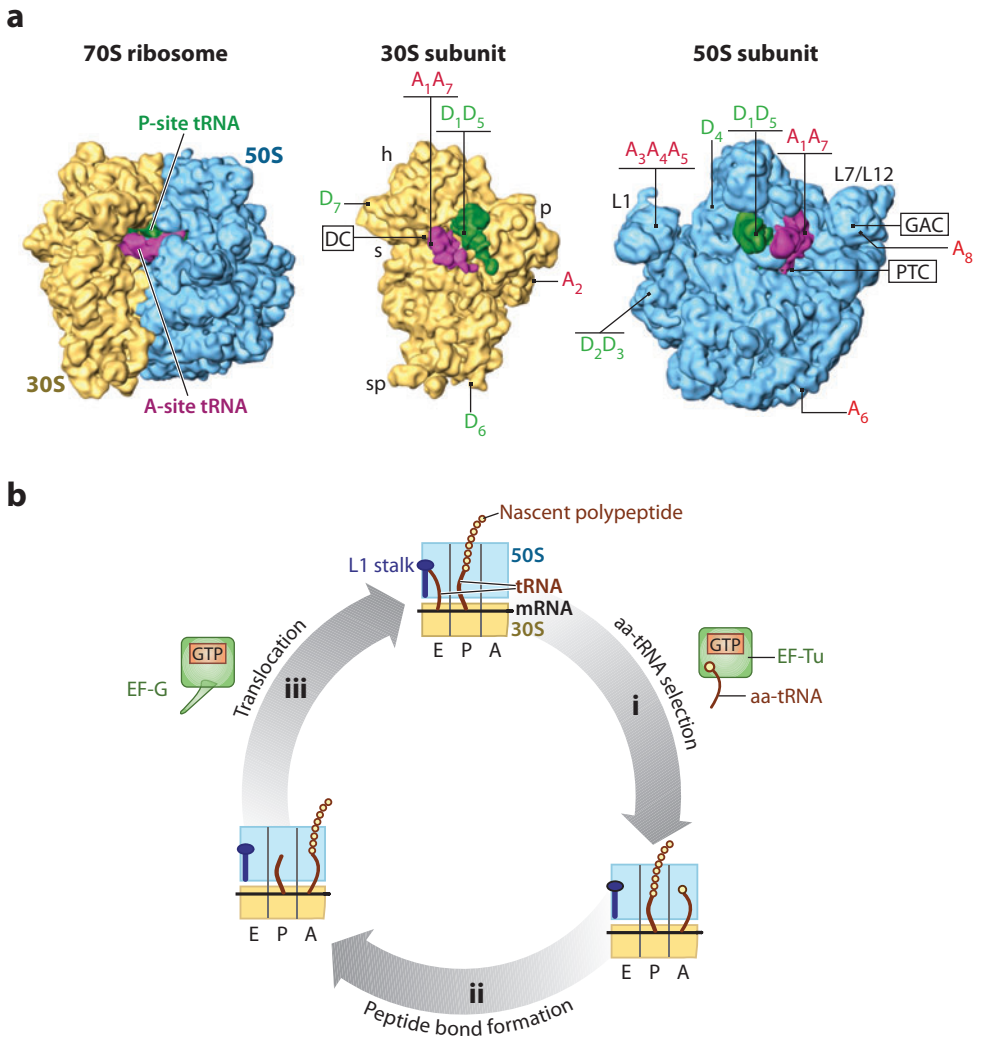

Figure 1

(*a*) Structure and dynamic features of the ribosome. Cryogenic electron microscopic map of the 70S ribosome, the 30S subunit, and the 50S subunit. The 30S and 50S subunits are shown with their intersubunit space facing the reader. The P- and A-site tRNAs are depicted in green and magenta, respectively, and their positions are denoted on the 70S ribosome. Major landmarks and mobile elements of the 30S subunit are the head (h), shoulder (s), platform (p), and spur (sp). The location of the decoding center (DC) active site is also denoted. Major landmarks and mobile elements of the 50S subunit are the L1 stalk (L1) and the L7/L12 stalk (L7/L12). The locations of the GTPase-associated center (GAC) and peptidyltransferase center (PTC) active sites are also denoted. The locations of all donor (D) and acceptor (A) fluorophore pairs that have thus far been used in single-molecule fluorescence resonance energy transfer investigations of translation elongation are labeled in green (D) and red (A). Details regarding each A-D pair are given in **Table 1**. (*b*) The elongation cycle of protein synthesis. The main steps of the translation elongation cycle, (*i*) aminoacyl-tRNA (aa-tRNA) selection, (*ii*) peptidyl transfer, and (*iii*) messenger RNA (mRNA)-tRNA translocation, are shown. The E, P, and A tRNA binding sites run vertically along both subunits. Further details regarding the mechanism of aa-tRNA selection and mRNA-tRNA translocation are provided in the captions for **Figures 2** and **3**, respectively. Abbreviations: EF, elongation factor.

Brownian motor: a biomolecular machine that rectifies or biases stochastic Brownian forces in the thermal bath to perform work

Translocation: movement of the messenger RNA and the A-site and P-site tRNAs through the ribosome by one codon

Free-energy landscape: plot of the free energy as a function of reaction and conformational coordinates

product away from a catalytic site. *Escherichia coli* RNA polymerase provides an excellent example of a well-studied molecular motor whose translocation is driven by a Brownian motor mechanism (8, 9). During the translocation step of the transcription elongation cycle, RNA polymerase has been observed to randomly oscillate between pre- and posttranslocation positions on the DNA template. Binding of nucleoside triphospate to the polymerase lowers the free energy of the forward position relative to the reverse position and thus imparts processivity to the polymerase.

An important aspect of Brownian motor function is the ability of the motor and its mechanical parts to undergo stochastic, thermally driven structural fluctuations. Indeed, it is the nanoscale dimensions of molecular motors and the energetically weak nature of the noncovalent interactions underlying their three-dimensional structures that permit biomolecular mechanical parts to operate at energies just above those available from the surrounding thermal bath. Brownian motors operate along a free-energy landscape in which fluctuations between two or more conformational states, such as the fluctuation of RNA polymerase between pre- and posttranslocation, are thermally accessible.

1.2. The Free-Energy Landscape of a Brownian Motor

Complex free-energy landscapes comprising numerous energy minima (valleys) and maxima (peaks) were originally introduced and developed in studies of protein (10, 11) and RNA folding (12–16). Viewed through this lens, an ensemble of protein or RNA molecules folds by navigating along a complex free-energy landscape, giving rise to multiple parallel folding pathways, locally stable folding intermediates, and kinetic trapping of the folding biopolymers (10–16). An excellent metaphor, provided by Dill & Chan (17), is that of water flowing along different routes down a collection of rugged hillsides that, despite experiencing different, trajectory-dependent physical obstacles to flow, ultimately collects at the same reservoir at the bottom of a deep valley. More recently, strong evidence has suggested that complex free-energy landscapes also underlie the catalytic cycles of various enzymes and ribozymes (18–28). In this view, individual enzymes or ribozymes within the ensemble can react via any one of numerous parallel reaction pathways. As the reaction proceeds, catalysis is guided by the differential stabilization (i.e., via ligand or substrate binding, product formation, and/or product release) of preexisting, thermally accessible, and on-pathway conformational intermediates. Although the role of enzyme or ribozyme conformational dynamics in guiding catalysis has been primarily developed using relatively simple model systems (18–28), it is quite likely that these ideas extend to catalysis in much more complex systems (29), including the mechanochemical cycles of Brownian motors.

1.3. Free-Energy Landscapes and the Concepts of States, Allosteric Regulation, and Induced Fit

The concept of a complex free-energy landscape forces a careful reconsideration of what is meant by the term state. The term state has often been colloquially used to refer to a single, relatively low-energy (i.e., stable) configuration of the molecule along the reaction trajectory. The corresponding picture is that of a linear progression of the entire system with defined points before and after. Contrasting with the concept of a state as a single, low-energy molecular configuration, increasing evidence supports the view that biomolecules (18–28), particularly complex biomolecular assemblies such as the ribosome (30, 31), are conformationally flexible and highly dynamic entities. Thus, states are much more adequately defined by reference to a complex free-energy landscape. Each valley in the landscape represents a free-energy minimum that is populated by an ensemble of conformations that collectively reflect a more-or-less stable state. The peaks separating the valleys represent energetic

barriers between the various states, and depending on the heights of these barriers relative to the available average thermal energy [$RT = 2.5$ kJ mol^{-1} at 298 K, where R is the universal gas constant (8.314 J K^{-1} mol^{-1}) and T is temperature], transitions between states may be either thermally driven or may require the energy released by a chemical reaction.

The exact depths of the valleys and heights of the barriers in the free-energy landscape are a function of numerous variables and can be readily altered, for example, by changes in buffer conditions; by the binding of a substrate, cofactor, or allosteric effector; and by mutation. Thus, the proportion of molecules found in the valleys under any given condition and the ability of molecules to cross a barrier into a neighboring state are sensitive functions of these variables. It is this capability to redistribute the conformational ensemble and alter the rate of interconversion among the various conformers that allows ligands to allosterically regulate enzyme or ribozyme activity. Because binding of a cofactor (or allosteric effector) at a regulatory site can control the accessibility and population of conformations over the entire enzyme's or ribozyme's molecular surface, catalytic or binding site geometries can be very effectively regulated, regardless of their distance from the regulatory site.

The conformational dynamics and existence of multiple pathways implied by a complex free-energy landscape also require a reassessment of the concept of induced fit. Studies using dihydrofolate reductase (18, 21), ribonuclease A (23), and reverse transcriptase and its inhibition (24) as model systems have revealed that dynamics in the micro- to millisecond time regime allow the system to sample productive binding configurations, even in the absence of the ligand. Thus, the phenomenon of induced conformational changes in molecular interactions termed induced fit (32, 33) is perhaps better described as a conformational selection (34, 35) or selected fit (36) mechanism (28), in which the ligand simply binds to and stabilizes a productive binding configuration of the biomolecule during the time interval in which that configuration is sampled.

1.4. Single-Molecule Studies of Protein Synthesis

Recent studies relating to the structural dynamics of the translational machinery are providing compelling evidence that Brownian motor mechanisms operating along a complex free-energy landscape may underlie one of nature's most fundamental and complex multistep biochemical processes: protein synthesis (reviewed in References 1, 3, 4). It is in this context that single-molecule approaches to connect cryo-EM and X-ray snapshots in real time have emerged as a powerful tool for investigating the mechanisms through which the translational machinery couples chemical events, such as factor-dependent GTP hydrolysis, release of inorganic phosphate, and peptidyl transfer, to the mechanical steps of protein synthesis (37–60). Single-molecule fluorescence resonance energy transfer (smFRET) experiments, in particular, are uncovering the important role that large-scale, thermally driven conformational fluctuations of the translational machinery play in regulating mechanical events during translation elongation (38–44, 47, 52–56, 58–60). In this review, we integrate a rapidly evolving series of findings by cryo-EM (61–69), X-ray (70–86), and smFRET (38–47, 51–56, 58–60) studies of translation elongation that are beginning to define the complex free-energy landscape underlying translation elongation. Our analysis strongly suggests that Brownian motor mechanisms lie at the heart of at least two of the principal steps in the elongation cycle: aminoacyl-transfer RNA (aa-tRNA) selection and translocation. By using these two examples to describe the emerging mechanistic themes and identify the remaining questions and challenges, we hope to stimulate further investigation of the hypothesis that similar Brownian motor mechanisms underlie many, if not all, of the individual steps of protein synthesis (2–4).

Peptidyl transfer: ribosome-catalyzed transfer of the nascent polypeptide chain from the P site-bound peptidyl-tRNA to the A site-bound aa-tRNA

Single-molecule fluorescence resonance energy transfer (smFRET): measurement of the energy transfer efficiency between donor and acceptor fluorophores on single molecules

Aminoacyl-transfer RNA (aa-tRNA) selection: selection of an aa-tRNA cognate to the codon at the ribosomal A site by the mRNA-programmed ribosome

2. THE STRUCTURAL AND DYNAMIC TOOLKIT

At present, the tools of choice for characterizing ribosome structure and dynamics are cryo-EM, X-ray crystallography, and smFRET. These three techniques provide complementary and interdependent experimental information that are collectively driving our rapidly evolving view of the role that ribosome structural dynamics play in the mechanism and regulation of protein synthesis. Below, we describe these three approaches, discuss each of their advantages and disadvantages, and emphasize how the complementarity and interdependence of these three techniques overcome their individual disadvantages. Our intent is to present a persuasive argument that the synergistic application of these methods will ultimately provide a virtual movie of protein synthesis by the ribosome.

2.1. Cryogenic Electron Microscopy

The technique of cryo-EM combined with single-particle reconstruction (see References 87 and 88) produces a three-dimensional density map from thousands of projections of different molecules ideally having identical structure, trapped in random orientations within a thin layer of ice. In contrast to X-ray crystallography (see below), the molecule is frozen in its native state, without constraints from functionally meaningless intermolecular contacts. **Figure 1*a*** introduces the ribosome as seen by cryo-EM, with landmarks and important mobile elements denoted. In the application of this technique to the ribosome, the challenge is to find ways to trap the majority of the molecules in the same state, usually by the addition of small-molecule, ribosome-targeting antibiotics or nonhydrolyzable GTP analogs. Dynamics can be inferred by comparing ribosome complexes captured in successive states (see Reference 89). Any residual heterogeneity in a sample poses a problem. However, new and powerful classification methods have made it possible to divide the data into homogeneous subsets. Frequently, therefore, a single sample results in two or more reconstructions, each for a subpopulation of molecules in a defined state (e.g., References 62 and 68).

As an ensemble average, a cryo-EM reconstruction has features with varying resolution, reflecting local variability of conformation. Peripheral components sticking out into the solvent, or components that are functionally mobile, may therefore appear washed out. However, the most serious drawback is that presently, with a few exceptions (molecules with high symmetry), the density maps are of insufficient resolution to allow chain tracing. Much effort has therefore gone into the development of so-called hybrid techniques, i.e., tools for interpreting medium-resolution density maps of molecular complexes in terms of atomic-resolution X-ray structures of their components. Some of the novel flexible fitting tools (e.g., Reference 90) yield structures that are intact, are sterochemically correct, and are in optimal agreement with the density restraints, even though they are not uniquely determined by them owing to insufficient resolution.

2.2. X-Ray Crystallography

X-ray crystallography, whose stunning achievements form the basis of all current structural interpretations of translation, shows the molecule confined and packed in a crystal, in a conformation not necessarily related to its function. In some cases, a gallery of structures of the same molecule in different crystals or even in the same unit cell (e.g., Reference 91) may hint at the range of accessible or functionally important conformations. However, care must be taken when inferring dynamics from such comparisons of X-ray crystallographic structures, as it has been noted that the constraints imposed by the crystal lattice are likely to dampen or inhibit the range and extent of conformational changes that are observed (74, 92). Moreover, ligands frequently have to be modified or truncated to allow crystal formation; for instance, tRNA has often been substituted by an anticodon stem loop (ASL)

(e.g., References 73 and 93), which limits the information one can gain about the way the intact tRNA interacts with the ribosome and how the intact tRNA might serve to transmit conformational events originating within the small 30S ribosomal subunit to the large 50S ribosomal subunit. Notably, X-ray crystallographic structures of elongation factor–bound ribosomes have recently emerged, allowing an atomic-resolution analysis of the interactions that these factors make with the ribosome during the elongation cycle (85, 86).

2.3. Single-Molecule Fluorescence Resonance Energy Transfer

Neither cryo-EM nor X-ray crystallography provides information on the evolving dynamic process itself. smFRET (94, 95) is uniquely suited to provide such information on a molecular motor in motion. smFRET draws directly from both cryo-EM and X-ray crystallography in the design of experiments (i.e., in the placement of donor and acceptor fluorophore pairs) for maximum information on dynamic distance changes associated with molecular function. In a rapidly evolving area of ribosome research, through careful positioning of donor-acceptor pairs, smFRET is providing real-time dynamic information on many of the structural rearrangements that have been inferred from comparisons of cryo-EM and X-ray structures (38–43, 44–46, 48, 51–60). **Figure 1*a*** and **Table 1** define the positions of all donor-acceptor pairs that have thus far been used in smFRET studies of translation.

Although smFRET provides time-resolved information on changes in molecular distances, typically only a single distance is monitored per donor-acceptor labeling scheme. Extension of

Table 1 Positions within the translational machinery that have been labeled with donor-acceptor fluorophore pairs in smFRET studies of translation elongation

Figure 1 designation	Donor fluorophore position	Acceptor fluorophore position	References
D_1/A_1	4-Thiouridine residue at position 8 of P-site $tRNA^{fMet}$	3-(3-Amino-3-carboxy-propyl) uridine residue at position 47 of A-site $tRNA^{Phe}$	38, 39, 44, 47, 52–56, 58, 59
	4-Thiouridine residue at position 8 of P-site $tRNA^{Phe}$	3-(3-Amino-3-carboxy-propyl) uridine residue at position 47 of A-site $tRNA^{Lys}$	52–54
D_2/A_2	C11 within an N11C single-cysteine mutant of ribosomal protein L9	C41 within a D41C single-cysteine mutant of ribosomal protein S6	43
D_3/A_3	C18 within a Q18C single-cysteine mutant of ribosomal protein L9	C202 within a T202C single-cysteine mutant of ribosomal protein L1	40, 60
D_4/A_4	C29 within a T29C single-cysteine mutant of ribosomal protein L33	C88 within an A88C single-cysteine mutant of ribosomal protein L1	42
D_5/A_5	3-(3-Amino-3-carboxy-propyl) uridine residue at position 47 of P-site $tRNA^{Phe}$	C202 within a T202C single-cysteine mutant of ribosomal protein L1	40, 41, 57, 60
	4-Thiouridine residue at position 8 of P-site $tRNA^{fMet}$	C55 within a S55C single-cysteine mutant of ribosomal protein L1	52, 53
	4-Thiouridine residue at position 8 of P-site $tRNA^{Phe}$	C55 within a S55C single-cysteine mutant of ribosomal protein L1	52, 53
D_6/A_6	Helix 44 of 16S rRNA (nucleotides 1450–1453)	Helix 101 of 23S rRNA (nucleotides 2853–2864)	45, 48
D_7/A_7	Helix 33a of 16S rRNA (nucleotides 1027–1034)	3-(3-Amino-3-carboxy-propyl) uridine residue at position 47 of A-site $tRNA^{Phe}$	51
D_8/A_8	C231 within an E231C single-cysteine mutant of EF-G	Unique native cysteine C38 within ribosomal protein L11	46

EF-Tu: elongation factor Tu

EF-G: elongation factor G

smFRET technology to simultaneously monitor two distances using three-color smFRET (i.e., using smFRET signals between one donor and two distinct acceptor fluorophores) within a single biomolecule has been recently reported (52, 53, 96, 97). However, the spectral properties required to generate appreciable energy transfer between the donor and both acceptors (and minimize the potentially complicating energy transfer between the two acceptors) are at odds with the spectral properties required to adequately detect the two resulting smFRET signals; thus, careful balancing of these opposing requirements (97) presents technical challenges [i.e., unacceptable amounts of donor or acceptor signal bleed through into the improper detection channel(s), very low signal-to-noise ratios, etc.] that often result in smFRET data that cannot be quantitatively analyzed (52, 53). Complicating matters further, the observed value of FRET efficiency is dependent on a number of spectroscopic and physical variables that must be carefully measured for each donor-acceptor labeling scheme in order to extract an accurate estimate of the distances between the donor and acceptor fluorophores (98). Therefore, relative to X-ray crystallography and cryo-EM, the structural resolution available from smFRET experiments is considerably limited, and the technique is best applied to obtain kinetic information on structural rearrangements that have already been well defined by comparisons of X-ray and/or cryo-EM structures. In the ideal smFRET experiment, donor and acceptor fluorophores are introduced into mobile and static structural elements of the ribosomal complex, respectively, such that the recorded smFRET data report on the intrinsic dynamics of the mobile element relative to a static landmark (39, 40, 42, 43, 45, 48, 51, 55, 56, 59, 60). smFRET studies where both fluorophores, or all three fluorophores in the case of three-color smFRET experiments, are positioned on mobile elements of the ribosomal complex are more difficult to interpret and often require prior knowledge, or a model, of the structural rearrangements that are being probed (38, 41, 44, 46, 52–54, 57, 58, 60).

Given the strengths and limitations of each of these techniques, the consensus is emerging that all three should be employed in the quest to understand the mechanism of protein synthesis (see for instance References 31 and 99). Indeed, the synthesis of cryo-EM, X-ray crystallography, and smFRET data has already yielded important insights into the mechanisms of aa-tRNA selection (39, 51, 55, 56, 59, 61, 64, 69, 73, 74, 85) and translocation (38, 40–43, 44–46, 52–54, 58, 60, 62, 63, 68, 86, 99, 100).

3. THE TRANSLATION ELONGATION CYCLE

The translation elongation cycle can be divided into three fundamental steps (**Figure 1*b***): (*a*) selection and incorporation of an aa-tRNA into the ribosomal A site, a step which is catalyzed by the essential GTPase elongation factor Tu (EF–Tu) (101); (*b*) peptidyl transfer of the nascent polypeptide from the peptidyl-tRNA at the ribosomal P site to the aa-tRNA at the A site, effectively deacylating the P-site tRNA and increasing the length of the nascent polypeptide now on the A-site tRNA by one amino acid (102); and (*c*) translocation of the ribosome along the messenger RNA (mRNA) template by precisely one codon and the accompanying joint movement of the newly deacylated tRNA from the P to the E site and the newly formed peptidyl-tRNA from the A to the P site, a step which is catalyzed by a second essential GTPase, elongation factor G (EF-G) (99, 103). At its conclusion, the translocation reaction places the subsequent mRNA codon at the A site such that the elongation cycle can be repeated for incorporation of the next mRNA-encoded amino acid.

3.1. Aminoacyl-tRNA Selection

aa-tRNA selection is a complex, multistep process during which an aa-tRNA, in the form of a ternary complex with elongation factor Tu (EF-Tu) and GTP, is selected by the ribosome from among at least 20 species of aa-tRNAs

as dictated by the mRNA codon presented at the A site. Successful recognition of a cognate aa-tRNA results in transmission of a conformational signal to EF-Tu that triggers GTP hydrolysis and subsequent domain rearrangement of the factor resulting in its dissociation and the accommodation of the aa-tRNA into the ribosome.

3.1.1. Kinetic proofreading, induced fit, and the fidelity of protein synthesis. **Figure 2** presents the mechanism of aa-tRNA selection as deduced from comprehensive biochemical kinetic experiments (101, 104); where available, cryo-EM snapshots of ribosomal complexes that appear along the reaction pathway are also depicted. aa-tRNA selection is a process in which a series of selection steps control the ability of the incoming aa-tRNA to participate in the peptidyltransferase reaction. It is within this series of selection steps that kinetic proofreading (105, 106) and induced-fit (101, 106, 107) mechanisms discriminate aa-tRNAs that are cognate to the mRNA codon at the A site from those that are near- or noncognate.

aa-tRNA arrives at the ribosome as part of a ternary complex with EF-Tu and GTP (step 0 → 1, **Figure 2**). Selection of aa-tRNA is based on Watson-Crick base-pairing between the mRNA codon and aa-tRNA anticodon (steps 1 → 3, **Figure 2**). Recognition of a cognate or, with a much lower probability, a near-cognate codon-anticodon complex (39, 59, 104) triggers GTP hydrolysis and release of inorganic phosphate from EF-Tu (steps 3 → 5, **Figure 2**). This is an irreversible event which separates the initial selection stage of aa-tRNA selection from the subsequent proofreading stage (steps 5 → 7, **Figure 2**), thus providing two independent opportunities to reject near-cognate aa-tRNAs. An important proposal stemming from the kinetic data is that the rates of GTP hydrolysis (k_4, **Figure 2**) and peptidyl transfer (k_7, **Figure 2**) are limited not by active-site chemistry, but rather by two preceding structural rearrangements of the ribosomal elongation complex termed GTPase activation (k_3/k_{-3}) and aa-tRNA accommodation ($k_6/k_{6'}$, **Figure 2**). Notably, induced-fit mechanisms synergistically enhance the fidelity established by kinetic proofreading through selectively accelerating GTPase activation (k_3, **Figure 2**) and accommodation (k_6, **Figure 2**) in response to cognate versus near-cognate aa-tRNAs.

DC: decoding center

GAC: GTPase-associated center

3.1.2. Codon recognition and 30S subunit domain closure. In structural terms, aa-tRNA selection begins with binding of EF-Tu to the L7/L12 stalk near the GTPase-associated center (GAC) (**Figure 1*a***) of the 50S subunit and the formation and recognition of the codon-anticodon complex at the decoding center (DC) within the A site of the 30S subunit. NMR studies of an RNA oligonucleotide mimic of a portion of the DC (108, 109) suggested that in the absence of ligands the DC is conformationally dynamic (109), a finding that holds true within the authentic, ligand-free DC in an intact 30S subunit (74).

Details concerning the nature of the codon-anticodon interaction and its recognition and stabilization by the DC have emerged from X-ray studies of the 30S subunit. By soaking mRNA fragments and tRNA ASLs into crystals of the isolated 30S subunit, Ramakrishnan and coworkers (74) have demonstrated that binding of a cognate codon-anticodon complex into the DC stabilizes a specific local conformation of the otherwise disordered DC, in which the universally conserved nucleotides A1492, A1493, and G530 stably associate with the cognate codon-anticodon complex. In addition, binding of a cognate codon-anticodon complex into the DC induces a global conformational change of the 30S subunit, termed domain closure, in which the head and shoulder domains (**Figure 1*a***) rotate toward the center of the 30S subunit (73).

Based on comparisons of the X-ray crystal structures, the 30S subunit domain closure has been described as a conformational change that is induced upon recognition of a cognate codon-anticodon complex. However, it is likely that the head and shoulder domains within states 0, 1, and 2 in **Figure 2** are

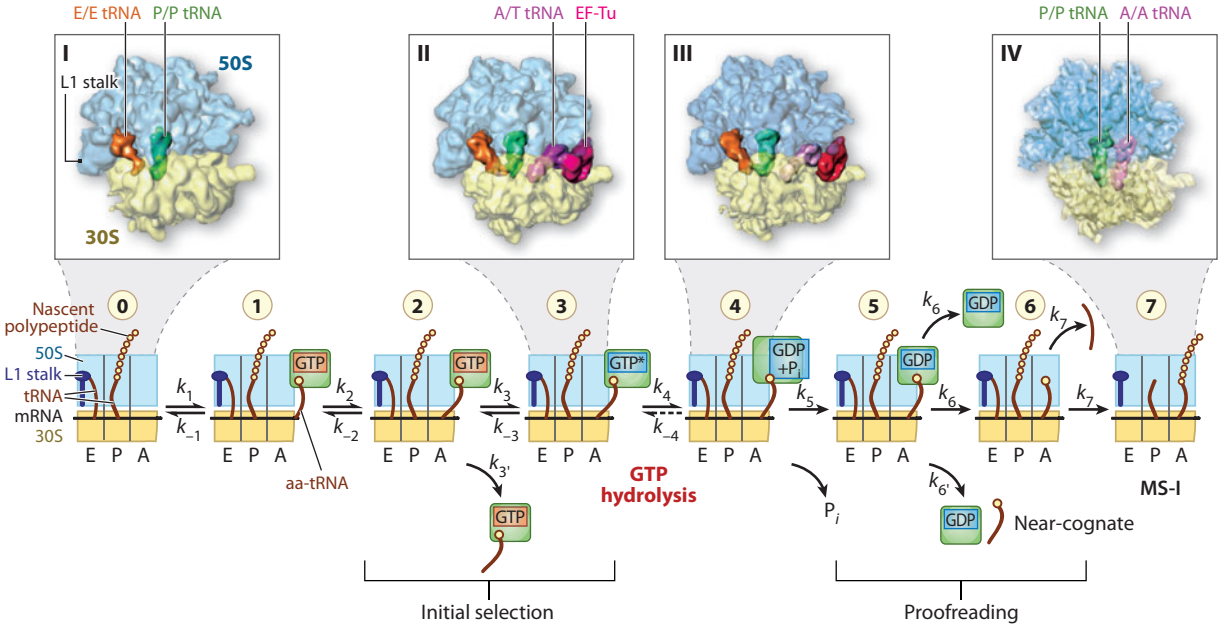

Figure 2

Distinct states and reversible/irreversible steps of the decoding and peptidyl transfer processes, and corresponding cryogenic electron microscopy (cryo-EM) maps, where available. In this schematic, tRNAs are colored according to their positions in the canonical (A, P, E) scheme, consistent with color choices in previous work [e.g. Reference (63)]. State 0: The posttranslocational state in which the A site is unoccupied, the P site contains a peptidyl-tRNA bound in the classical P/P (denoting the 30S P/50S P sites, respectively) configuration, and the E site contains a deacylated tRNA bound in the classical E/E configuration and in direct contact with the open L1 stalk. (Note: The E-site tRNA contacts the L1 stalk through its central fold, or elbow, domain.) Cryo-EM map *I* from Valle and coworkers (63). Step 0 → 1 (reversible; k_1/k_{-1}): The binding of elongation factior Tu (EF-Tu) in a ternary complex with aminoacyl-tRNA (aa-tRNA) and GTP to the ribosome via the L7/L12 stalk. State 1: The same as state 0 but with ternary complex bound to ribosome. Step 1 → 2 (reversible; k_2/k_{-2}): The probing of the mRNA codon by the aa-tRNA anticodon at the decoding center (DC). State 2: The same as state 1 but the aa-tRNA anticodon is engaged with the codon at the DC. Step 2 → 3 (reversible; k_3/k_{-3}): The cognate and a fraction of near-cognate ternary complexes are bound sufficiently long to induce GTPase activation of EF-Tu. Step 2 → 3 (irreversible; $k_{3'}$): The noncognate and a fraction of near-cognate ternary complexes are rejected as their binding to the ribosome fails to stabilize. State 3: The same as state 2 but with EF-Tu activated for GTP hydrolysis. Cryo-EM map *II*: The use of guanylyl iminodiphosphate prevents GTP hydrolysis (119; J. Sengupta, O. Kristensen, F. Fabiola, H. Gao, M. Valle, et al., in preparation). Step 3 → 4: (reversible; k_4/k_{-4}) GTP hydrolysis on EF-Tu. State 4: The same as state 3 but with EF-Tu bound in the GDP-P_i state. Cryo-EM map *III*: After GTP hydrolysis, kirromycin prevents conformational change of EF-Tu and locks the ternary complex in the A/T configuration (64). Step 4 → 5 (irreversible; k_5): The departure of P_i. State 5: The same as state 4 but with EF-Tu bound in the GDP only state. Step 5 → 6 (irreversible; k_6): The conformational change of EF-Tu, departure of EF-Tu·GDP, and accommodation of cognate aa-tRNA. (irreversible; $k_{6'}$): The conformational change of EF-Tu, departure of EF-Tu·GDP, and departure of near-cognate aa-tRNA. State 6: The same as state 5, but with aa-tRNA accommodated in the classical A/A configuration within the A site. Step 6 → 7 (irreversible; k_7): The departure of E-site tRNA and peptidyl transfer. (Note that the precise timing of the E-site tRNA departure has not been established, so this placement is tentative.) State 7: The macrostate I form of the pretranslocational complex is the same as state 6 but the nascent polypeptide is now covalently linked to the A-site tRNA, whereas the P-site tRNA is deacylated, and the E site is unoccupied. The ribosome is in its nonrotated conformation, the tRNAs are in their classical A/A and P/P positions, and the L1 stalk is in its open conformation. Cryo-EM map *IV* from Agirrezabala and coworkers (68).

inherently conformationally dynamic and that binding of a cognate codon-anticodon complex into the DC simply selectively stabilizes the global conformer that is observed in the X-ray studies. Indeed, the observation that, depending on experimental conditions, the ribosome has anywhere from a 1 in 1×10^3 (110, 111) through a 1 in 1×10^5 (112, 113) probability

of misincorporating a near-cognate aa-tRNA suggests that binding of a near-cognate codon-anticodon complex into the DC has some probability of inducing or selectively stabilizing the domain-closed form of the 30S subunit.

Structural clues regarding how the domain closure event, inferred from X-ray studies of the isolated 30S subunit, might couple recognition of a cognate codon-anticodon complex at the DC to activation of GTP hydrolysis on EF-Tu at the GAC of the 50S subunit come from structural studies of ternary complex binding to ribosomes in the presence either of the nonhydrolyzable GTP analog, guanylyl iminodiphosphate (GDPNP), or of the antibiotic kirromycin. Kirromycin is a small-molecule antibiotic, which is known to block the aa-tRNA selection process at a step following GTP hydrolysis but prior to the conformational change of EF-Tu that normally results in its dissociation from the ribosome and the release of the aa-tRNA acceptor stem (114, 115). Recognition of a cognate or, with much lower probability, a near-cognate codon-anticodon complex at the DC leads to formation of the so-called A/T configuration of the ternary complex, a transient configuration visualized by cryo-EM (61, 64, 66, 69, 116–118) and, more recently, by X-ray crystallography (85), in which the aa-tRNA anticodon engages the codon at the DC while the aa-tRNA acceptor stem remains bound to EF-Tu (map *II*, **Figure 2**). The structures of the kirromycin-stabilized A/T configuration have not only pinned down the intermolecular contacts between EF-Tu and the ribosome but also demonstrated that, upon EF-Tu binding, the L11 stalk (**Figure 1*a***), which forms part of the GAC, curls inward toward the peptidyltransferase center (PTC) (**Figure 1*a***) of the 50S subunit (64, 85, 117, 119). Perhaps most importantly, the structure of the A/T configuration led to the discovery of a large conformational change of the tRNA body, as compared to its known X-ray structure (120). Apparently, this conformational change, characterized as a kink and twist in the anticodon stem, permits a geometry in which the aa-tRNA acceptor stem can remain bound to EF-Tu while the anticodon stem can continue probing the codon-anticodon interaction (61, 64, 69, 85). It has been suggested, as we point out below, that the unusual conformation of the aa-tRNA may have a role in the kinetic proofreading step.

Guanylyl iminodiphosphate (GDPNP): a GTP nonhydrolyzable analog

3.1.3. The frequency and rate of stably forming the A/T configuration depend on codon-dependent fluctuations of the ribosome-bound ternary complex. Dynamic information connecting the recognition of the codon-anticodon complex at the DC, and presumably the associated 30S subunit domain closure event, with formation of the A/T configuration comes from smFRET studies of aa-tRNA selection. Using an smFRET signal between a donor-labeled P-site peptidyl-tRNA and an acceptor-labeled incoming aa-tRNA (D_1/A_1, **Figure 1*a*** and **Table 1**), delivery of a cognate ternary complex to the ribosome generated a rapidly evolving, presteady-state smFRET signal that started at a 0-FRET value prior to ternary complex binding and concluded at a high-FRET value once aa-tRNA was fully accommodated into the A site (steps $0 \rightarrow 6$, **Figure 2**) (39). In contrast with this result, delivery of a near-cognate ternary complex yielded multiple reversible fluctuations between the 0-FRET value and a novel low-FRET value, which reports on the transient binding of the ternary complex to the ribosome (steps $0 \rightleftarrows 2$, **Figure 2**). Interestingly, delivery of a noncognate ternary complex failed to yield any detectable smFRET signal, demonstrating that transient binding of noncognate ternary complex either does not take place or is unobservable using this particular fluorophore labeling scheme and/or available time resolution. The transient binding configuration of the ternary complex that is characterized by the low-FRET value, therefore, is one in which the DC is able to inspect and recognize the codon-anticodon complex (state 2, **Figure 2**). Although the configuration of the ternary complex associated with the low-FRET value is a critical intermediate in the aa-tRNA selection pathway, the stochastic and transient nature with which it is sampled makes it very difficult

to structurally characterize or biochemically investigate using ensemble experiments.

Steps along the smFRET trajectory that lie beyond the low-FRET, codon-dependent sampling of the DC can be investigated by substituting GTP with GDPNP in a manner analogous to the cryo-EM studies described above (39, 59). A cognate ternary complex delivered in the presence of GDPNP progresses through the low-FRET value and subsequently stabilizes at a mid-FRET value that directly corresponds to the A/T configuration visualized by cryo-EM (steps 0 → 3, **Figure 2**). Near-cognate ternary complexes, which are very effectively rejected from the configuration associated with the low-FRET value (steps 0 ⇄ 2, **Figure 2**), have a very low probability of stably achieving the A/T configuration associated with the mid-FRET value. Thus, the low- → mid-FRET transition reports on a codon-dependent structural rearrangement of the ribosome-bound ternary complex in which the aa-tRNA is brought closer to the peptidyl-tRNA (hence the increase in FRET) (step 2 → 3, **Figure 2**). This conformational change precedes GTP hydrolysis by EF-Tu, and its end point coincides with stable repositioning of EF-Tu at the GAC such that GTP hydrolysis by EF-Tu can be activated. It is therefore likely that the aa-tRNA itself participates in transmitting the codon-anticodon recognition signal from the DC to the GAC, inducing GTP hydrolysis by EF-Tu, in keeping with the results of tRNA cleavage (121) and mutational (122–124) studies.

Careful analysis of a large number of smFRET trajectories reveals that both cognate and near-cognate ternary complexes can fluctuate reversibly between the low- and mid-FRET states (i.e., low- ⇄ mid-FRET) in the presence of GDPNP (59). In addition, two subpopulations of low- → mid-FRET transitions were detected. One subpopulation remains at the mid-FRET value transiently, rapidly transiting back to the low-FRET value. This subpopulation likely represents unsuccessful attempts of the ternary complex to reposition at the GAC, an interpretation that is supported by similar smFRET experiments performed in the presence of the small-molecule, GAC-targeting antibiotic thiostrepton (56). The second population exhibits a stable and long-lived mid-FRET signal that indicates the successful repositioning of the ternary complex at the GAC. These data directly report on stochastic, thermally driven fluctuations of the ternary complex between configurations characterized by low- and mid-FRET values. Comparison of cognate and near-cognate ternary complex delivery in the presence of GDPNP demonstrates that near-cognate ternary complexes are ~sixfold less likely to undergo a low- → mid-FRET transition, exhibit a ~threefold decrease in the rate of low- → mid-FRET transitions, and are ~twofold less likely to undergo a successful versus an unsuccessful low- → mid-FRET transition. Thus, as part of the initial selection stage of aa-tRNA selection, thermally driven low- ⇄ mid-FRET fluctuations of the ribosome-bound ternary complex are biased in favor of cognate over near-cognate ternary complexes. If one assumes that low- → mid- and mid- → low-FRET transitions correspond to 30S domain closing and opening events, respectively, it is possible that rather than triggering a single, discrete 30S subunit domain closure event, recognition of a cognate codon-anticodon complex at the DC simply biases thermally driven open ⇄ closed fluctuations of the 30S head and shoulder domains. It would therefore be of great interest to design donor-acceptor pairs that directly report on the dynamics of the 30S subunit domain closure.

3.1.4. aa-tRNA distortion and fluctuations might drive and regulate the outcome of the accommodation reaction. Successful repositioning of a cognate and, with some probability, a near-cognate ternary complex at the GAC leads to GTPase activation (step 0 → 3, **Figure 2**) and GTP hydrolysis (step 3 → 4, **Figure 2**) on EF-Tu. The mechanism of GTPase activation of EF-Tu has been recently illuminated by two cryo-EM reconstructions of the A/T ternary complex configuration stabilized in the GDP-bound conformation using

the antibiotic kirromycin (61, 69). These two recent cryo-EM reconstructions demonstrate that successful repositioning of EF-Tu at the GAC triggers opening of a hydrophobic gate within EF-Tu, which allows a crucial EF-Tu histidine residue to reorient toward GTP and activate a water molecule, subsequently leading to GTP hydrolysis. These findings have been recently confirmed at atomic resolution using X-ray crystallography (85). Upon GTP hydrolysis and release of the resulting inorganic phosphate (steps 4 → 5, **Figure 2**), EF-Tu undergoes a large conformational change, which results in the above-described dissociation of EF-Tu·GDP from the ribosome and the release of the aa-tRNA acceptor stem (steps 5 → 6, **Figure 2**). At this stage, a near-cognate aa-tRNA is preferentially released from the ribosome ($k_{6'}$) while a cognate aa-tRNA, on account of its optimal binding stability at the DC, is preferentially accommodated into the PTC (k_6). Assuming that aa-tRNA in its kinked, twisted conformation is in a high-energy configuration, the stability of its binding interactions at the DC may set the threshold for selection (125). The mid- → high-FRET transition observed in presteady-state smFRET studies of aa-tRNA selection reports directly on the dynamics of aa-tRNA as it is accommodated from its position within the A/T configuration of the ternary complex into the PTC (39). Interestingly, rapid mid- ⇄ high-FRET fluctuations are observed when the A/T configuration is stabilized either by GDPNP or by GDP·kirromycin (39). This observation suggests that even prior to GTP hydrolysis, release of inorganic phosphate, or the subsequent conformational change of EF-Tu, aa-tRNA can fluctuate and transiently sample the high-FRET, fully accommodated state but that stable accommodation of aa-tRNA into the PTC might require additional conformational processes at the PTC that are somehow coupled to the conformational change and/or dissociation of EF-Tu from the ribosome. Thus, in a manner analogous to the initial selection stage of aa-tRNA selection, these results suggest that the proofreading stage of aa-tRNA selection involves thermally driven fluctuations of the tRNA from its binding site on EF-Tu into the PTC that are biased to favor cognate over near-cognate tRNAs.

3.2. Peptidyl Transfer

Owing to their current spatial and time resolution limits, cryo-EM and smFRET have not significantly contributed to our structural and dynamic understanding of the peptidyltransferase reaction. There is, however, significant biochemical (126–128) and X-ray structural (70) evidence strongly suggesting that local structural rearrangements of the PTC regulate the conversion of the catalytic center of the ribosome from an inactive conformation to a conformation that supports the peptidyl-transfer reaction. X-ray crystallographic structures of the 50S subunit bound to various analogs of peptidyl- and aa-tRNA acceptor stems, as well as a peptidyltransferase transition state analog, suggest that docking of the acceptor end of aa-tRNA into the PTC triggers a coupled structural rearrangement of the PTC and the acceptor ends of the peptidyl- and aa-tRNAs. The resulting conformation of the substrate-bound PTC exposes the reactive carbonyl group at the C-terminal end of the peptidyl-tRNA, optimally positioning it and the α-NH_2 group of the incoming aa-tRNA for the in-line nucleophilic attack that transfers the nascent polypeptide from the P site–bound peptidyl-tRNA to the A site–bound aa-tRNA (70). Results of studies using analogs of peptidyl- and aa-tRNA acceptor stems within the isolated 50S subunit have recently been supported by similar studies using full-length peptidyl- and aa-tRNA analogs within intact, 70S ribosomes (129).

3.3. mRNA-tRNA Translocation

After peptidyl transfer, the A-site tRNA within the pretranslocation (PRE) ribosomal complex carries the nascent polypeptide chain while the P-site tRNA is deacylated. mRNA and tRNAs must now be advanced such that the next codon is placed into the DC of the posttranslocation

(POST) ribosomal complex (**Figure 3**). This is accomplished with the aid of EF-G·GTP, which binds to the PRE complex in a position similar to that of the ternary complex (63, 67, 85, 86, 130, 131). Evidently the need to transport mRNA and two tRNAs by the span of a codon (~13 Å) requires large, coordinated conformational changes of the PRE complex

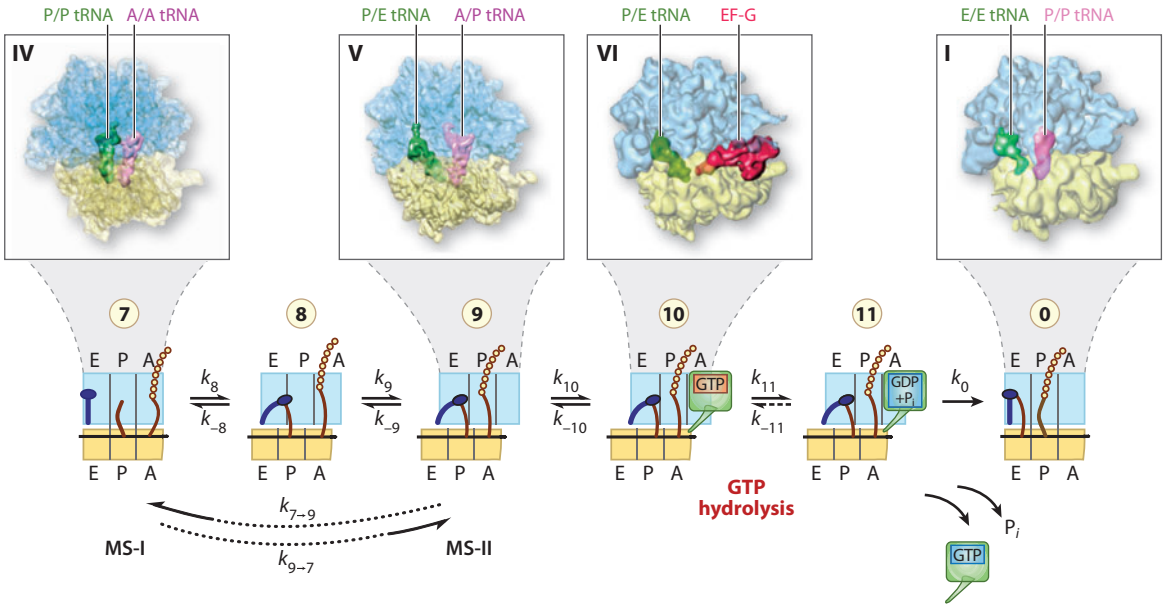

Figure 3

Distinct states and reversible/irreversible steps of the translocation process and corresponding cryo-EM maps, where available. In this schematic, unlike **Figure 2**, colors mark individual tRNAs, so that the steps of their translocation can be followed. State 7: The macrostate I (MS-I) form of the pretranslocational (PRE) complex is the same as state 7 in **Figure 2**. The A site contains the newly formed peptidyl-tRNA, the P site contains a deacylated tRNA, and the E site is unoccupied. The ribosome is in its nonrotated conformation, the tRNAs are in their classical A/A (denoting the 30S A/50S A sites, respectively) and P/P positions, and the L1 stalk is in its open conformation. Cryo-EM map *IV* from Agirrezabala and coworkers (68). Step 7 → 8 (reversible; k_8/k_{-8}): The rearrangement of MS-I into an intermediate state of ratcheting (44). State 8: This is the same as state 7 but with the PRE complex in an intermediate state of ratcheting consisting of a ribosome in a semirotated state and tRNAs in an intermediate classical A/A, hybrid P/E configuration that lies somewhere between the classical A/A and P/P configuration and the hybrid A/P and P/E configuration. The L1 stalk is in a "closed" position, where it forms a direct intermolecular contact with the hybrid P/E tRNA (44, 156). Step 8 → 9 (reversible; k_9/k_{-9}): The rearrangement of the intermediate state of ratcheting to macrostate II (MS-II) (44). State 9: The MS-II form of the PRE complex is the same as in state 8 but with the ribosome in the rotated state, tRNAs in hybrid A/P and P/E configurations, and the L1 stalk in a closed conformation where it directly contacts the hybrid P/E tRNA elbow. Cryo-EM map *V* from Agirrezabala and coworkers (68). Note: State 9 can alternatively be reached directly from state 7, bypassing the intermediate state 8. Step 9 → 10 (reversible; k_{10}/k_{-10}): The binding of EF-G in the GTP state. State 10: The same as in state 9 but with EF-G bound in GTP state, stabilizing MS-II. Cryo-EM map *VI* from Valle and coworkers (63). Note that EF-G in the presence of guanylyl iminodiphosphate stably binds only to ribosomes with an unoccupied A site (63, 68). Step 10 → 11 (reversible; k_{11}/k_{-11}): GTP hydrolysis on EF-G. State 11: The same as state 10 but with EF-G bound in the GDP-P_i state. Step 11 → 0 (irreversible; k_0): The ribosome returns to the nonrotated position, the newly formed peptidyl-tRNA and the newly deacylated tRNA move into the classical P/P and E/E configurations, respectively, and the L1 stalk moves into the open position. EF-G·GDP and P_i depart from the ribosome. State 0: The posttranslocation complex. The same as in state 11 but with the ribosome in the nonrotated position, the newly formed peptidyl-tRNA and the newly deacylated tRNA in classical P/P and E/E configurations, respectively, and the L1 stalk in the open position. Cryo-EM map *I* from Valle and coworkers (63). [Note that using fusidic acid, EF-G has also been trapped on the ribosome in the GDP state, with the ribosome in the nonrotated position, the newly formed peptidyl-tRNA and the newly deacylated tRNA in classical P/P and E/E configurations, respectively, and the L1 stalk in the open position as depicted in state 0 (see References 63 and 86).] For clarity, we have refrained from adding a panel depicting this configuration.

(steps 7 → 0, **Figure 3**). Indeed, the PRE complex transitions from one major conformation, termed macrostate-I (MS-I) (99) or global state 1 (GS-1) (41), to a second major conformation, termed macrostate-II (MS-II) (99) or global state 2 (GS-2) (steps 7 → 9, **Figure 3**) (41), prior to stable binding of EF-G (step 9 → 10, **Figure 3**); throughout this article, we use the term macrostates or MS. The MS-I → MS-II transition is characterized by, among other structural rearrangements, a counterclockwise ratchet-like rotation of the 30S subunit relative to the 50S subunit (denoted hereafter as the nonrotated → rotated ribosome transition), which was first observed by Frank & Agrawal (30) by comparing cryo-EM maps, confirming early proposals by Bretscher (132) and Spirin (133) that an intersubunit rotation is employed in mRNA-tRNA translocation.

Formation of the hybrid A/P (denoting the 30S A/50S P sites, respectively) and P/E configurations of the ribosome-bound tRNAs (denoted hereafter as the classical → hybrid tRNA transition), originally inferred from chemical modification studies by Moazed & Noller (134) and subsequently confirmed by Hardesty and coworkers (135) using ensemble FRET, is intricately linked with intersubunit rotation and is thus also observed to occur as part of the MS-I → MS-II transition (62, 68, 136, 137). In addition to intersubunit rotation and formation of the hybrid tRNA configurations, the MS-I → MS-II transition also encompasses a closing of the ribosomal L1 stalk (**Figure 1*a***), a highly mobile domain within the 50S subunit (denoted hereafter as the open → closed L1 stalk transition) (40–42, 63, 71, 72, 77, 83, 91, 138–142), and formation of an intermolecular contact between the closed L1 stalk and the hybrid P/E tRNA (denoted hereafter as the L1◦tRNA → L1•tRNA transition) (30, 63).

According to a general rule recognized by Zavialov & Ehrenberg (143) and Valle et al. (63), the MS-I → MS-II transition does not take place unless the P-site tRNA is deacylated, a feature of the conformational dynamics of the ribosomal elongation complex that can be rationalized by the need to stabilize the ribosome's conformation during aa-tRNA selection. This rule is appropriately described as a locking/unlocking mechanism—in the sense that the unlocking of a door is necessary but not sufficient for the door to open. In the present case, the deacylation of the P-site tRNA only provides the precondition for the MS-I → MS-II transition.

Ribosome-stimulated GTP hydrolysis by EF-G and subsequent release of inorganic phosphate then causes EF-G to undergo a conformational change into the GDP form (86, 100), resulting in several interrelated events: decoupling of the mRNA-tRNAs complex from the DC (100), rotation of the 30S subunit head domain (91, 100, 131, 144), reversion of the rotation of the 30S subunit associated with intersubunit rotation (86, 99, 100), full advance of the next untranslated codon into the DC, and release of EF-G·GDP from the ribosome (steps 10 → 0, **Figure 3**). Head domain rotation and reverse rotation of the 30S subunit have been recognized as the steps leading to mRNA-tRNA translocation relative to the 30S subunit (99, 100).

3.3.1. Thermally driven, spontaneous fluctuations of pretranslocation complexes between macrostates I and II. Initially, binding of EF-G to the PRE complex was thought to be required to bring about the MS-I → MS-II transition, including the associated classical → hybrid tRNA transition, as this was the condition under which the original cryo-EM observations were made (30, 63). This result, however, was at odds with the chemical modification studies of Moazed & Noller (134) and ensemble FRET studies of Hardesty and coworkers (135), which indicated that the classical → hybrid tRNA transition occurs spontaneously upon peptidyl transfer and in the absence of EF-G. The notion that the classical → hybrid tRNA transition within a PRE complex might be a reversible process was first suggested by Green and coworkers (145) as a possible resolution of the discrepancies between the chemical modification (134) and ensemble FRET (135) studies, on the one hand,

Macrostates (MS-I and MS-II): two states of the ribosome that are encountered in the process of translocation and are characterized by major conformational rearrangements

Ratchet-like rotation: counterclockwise rotation of the small subunit with respect to the large subunit, leading from macrostate I to macrostate II

and the cryo-EM studies (30, 63), on the other. A few months later, the laboratories of Chu and Puglisi (38) reported the first smFRET investigation of tRNA dynamics within a PRE complex. Using the same tRNA-tRNA labeling scheme that was used in the smFRET studies of aa-tRNA selection (D_1/A_1, **Figure 1*a*** and **Table 1**), these studies directly demonstrated the reversible nature of the classical → hybrid tRNA transition, revealing that tRNAs within a PRE complex fluctuate stochastically between classical and hybrid configurations with free energies of activation, $\Delta G^{\ddagger}$, for the classical → hybrid transition of ~69 kJ mol^{-1} ($T = 296$ K) and for the hybrid → classical transition of ~70 kJ mol^{-1} ($T = 296$ K)—values that are, somewhat surprisingly, ~28-fold larger than the average thermal energy available at room temperature ($RT = 2.5$ kJ mol^{-1} at 296 K) (38).

The possibility that the tRNA fluctuations observed by Chu, Puglisi, and coworkers (38) might be accompanied by fluctuations of the entire PRE complex between the structurally observed MS-I and MS-II states in the absence of EF-G, as proposed by Kim et al. (58), suggested that a Brownian motor mechanism might underlie the translocation reaction, at least with respect to translocation of the tRNA acceptor ends within the 50S subunit. Initial experimental evidence suggesting that PRE complexes might spontaneously occupy the MS-II state in the absence of EF-G came from ensemble experiments in which an intersubunit FRET signal was used to demonstrate that PRE complexes could occupy the rotated ribosome conformation in the absence of EF-G (137). Direct experimental evidence suggesting that PRE complexes might fluctuate stochastically between the structurally observed MS-I and MS-II states in the absence of EF-G came from characterizing a variety of smFRET signals reporting directly on nonrotated and rotated ribosome conformations (D_2/A_2, **Figure 1*a***, and **Table 1**) (43), the open and closed L1 stalk conformations (D_3/A_3 and D_4/A_4, **Figure 1*a***, and **Table 1**) (40, 42, 60), and the formation and disruption of the L1 stalk-P/E tRNA intermolecular contact (D_5/A_5, **Figure 1*a***, and **Table 1**) (40, 41, 52, 60). Each of these individual smFRET signals has been found to stochastically fluctuate between two major states consistent with the MS-I and MS-II cryo-EM structures, thus defining individual nonrotated ⇄ rotated ribosome, open ⇄ closed L1 stalk, and L1∘tRNA ⇄ L1•tRNA dynamic equilibriums that, together with the classical ⇄ hybrid tRNA equilibrium, collectively define an MS-I ⇄ MS-II equilibrium.

Interestingly, data using a second intersubunit smFRET signal (D_6/A_6, **Figure 1*a*** and **Table 1**) were inconsistent with stochastic nonrotated ⇄ rotated fluctuations within a PRE complex (45). Instead, this study suggested that, during the elongation cycle, the energy of peptide bond formation drives the nonrotated → rotated transition, whereas the energy of ribosome-stimulated GTP hydrolysis on EF-G drives the reverse rotated → nonrotated transition. An alternative interpretation, however, that would reconcile the data obtained using the D_2/A_2 and D_6/A_6 intersubunit labeling schemes is that the D_6/A_6 labeling scheme simply reports on an as yet undefined conformational switch that is uniquely triggered upon each unlocking event (i.e., upon deacylation of the P-site tRNA) and uniquely reset upon each locking event (i.e., upon placement of the next peptidyl tRNA into the P site). Such a conformational switch need not directly correspond to, nor report on, the nonrotated ⇄ rotated fluctuations that are associated with the MS-I ⇄ MS-II equilibrium and that are reported on by the D_2/A_2 labeling scheme. Thus, the conformational cycle observed using the D_6/A_6 labeling scheme might report directly on the cycle of unlocking and locking that occurs during each round of the elongation cycle (146).

In complete agreement with the ensemble and smFRET investigations, two recent cryo-EM studies (62, 68), one of which was specifically performed under experimental conditions that alter the free-energy landscape of the MS-I ⇄ MS-II equilibrium (see Section 3.3.3. and **Figures 4** and **5**) in order to significantly populate MS-II (i.e., lower [Mg^{2+}], and **Figure 5**) (58, 68), were able

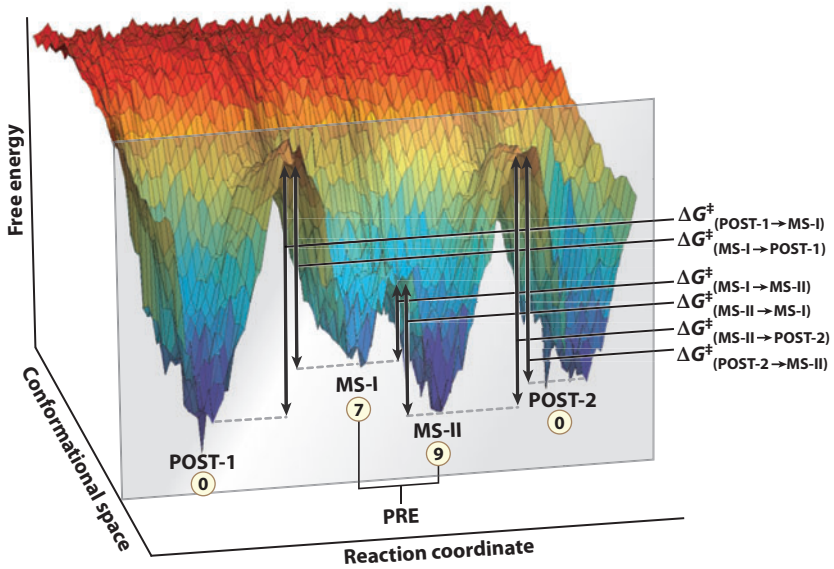

Figure 4

A heuristic schematic of the complex free-energy landscape of the elongation cycle, including macrostate (MS)-I and MS-II of the pretranslocational (PRE) ribosomal complex. Conformational changes of the ribosomal complex can occur along either the reaction coordinate or the conformational space axes. Conformational changes that take place along the reaction coordinate axis correspond to the rearrangements of the ribosomal complex that facilitate the elongation reaction that will ultimately transform posttranslocation (POST)-1 into POST-2. Conformational changes along the conformational space axis, by contrast, correspond to fluctuations among the ensemble of conformers that exist at all points along the reaction coordinate, leading to the availability of numerous parallel reaction pathways, which are the hallmark of a complex free-energy landscape. The energetic barriers separating POST-1 from the MS-I state of the PRE complex and the MS-II state of the PRE complex from POST-2 are large enough such that overcoming these barriers generally requires the energy released from GTP hydrolysis by elongation factor Tu and/or peptidyl transfer (for POST-1 → MS-I transitions) and GTP hydrolysis by EF-G (for MS-II → POST-2 transitions). The energetic barrier separating MS-I from MS-II, however, is small enough such that stochastic, thermally driven fluctuations between MS-I and MS-II are permitted. In addition, the ruggedness of the landscape strongly suggests that the valleys defining POST-1, MS-I, MS-II, and POST-2 are themselves composed of a multiplicity of smaller valleys separated by barriers even smaller than that separating MS-I from MS-II. Thus, POST-1, MS-I, MS-II, and POST-2 are each expected to be composed of an ensemble of conformations, with the population of any one member of the ensemble depending on the exact depth of its valley and heights of the barriers separating it from its neighbors. As experimentally demonstrated in **Figure 5**, the depth of the valleys within POST-1, MS-I, MS-II, and POST-2, as well as the depths of the POST-1, MS-I, MS-II, and POST-2 valleys themselves, are sensitive functions of environmental conditions (e.g., substrate, cofactor, or allosteric effector binding) or the dissociation of reaction products. The circled numbers listed underneath the POST-1, MS-I, MS-II, and POST-2 valleys refer to the equivalently labeled POST, MS-I, and MS-II complexes depicted in **Figure 3**. Abbreviation: $\Delta G^{\ddagger}$, free energy of activation.

to apply particle classification methods to single PRE complex samples in order to reveal the existence of two classes of particles with structures corresponding to MS-I and MS-II.

The structural rearrangements encompassed by MS-I ⇄ MS-II transitions are undoubtedly complex, involving substantial local as well as global reconfigurations of intra- and intersubunit ribosome-ribosome and ribosome-tRNA interactions (reviewed in Reference 31). Despite the complexity of these structural rearrangements, however, the

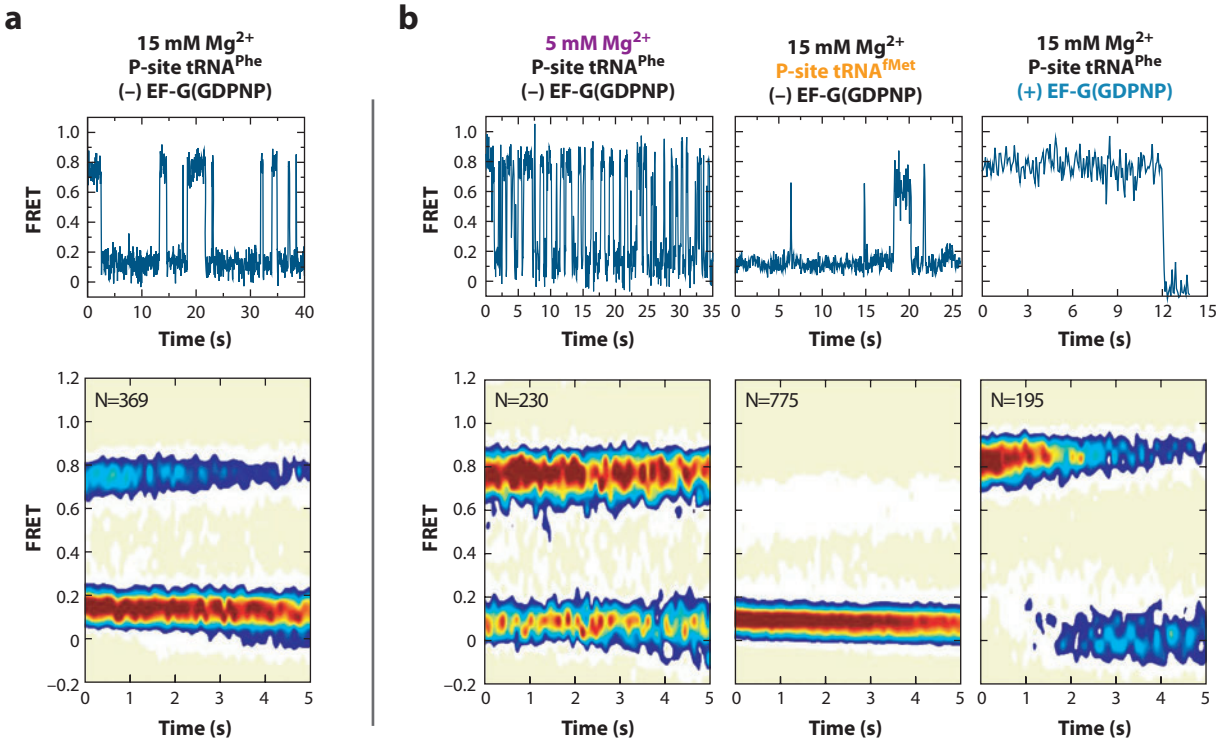

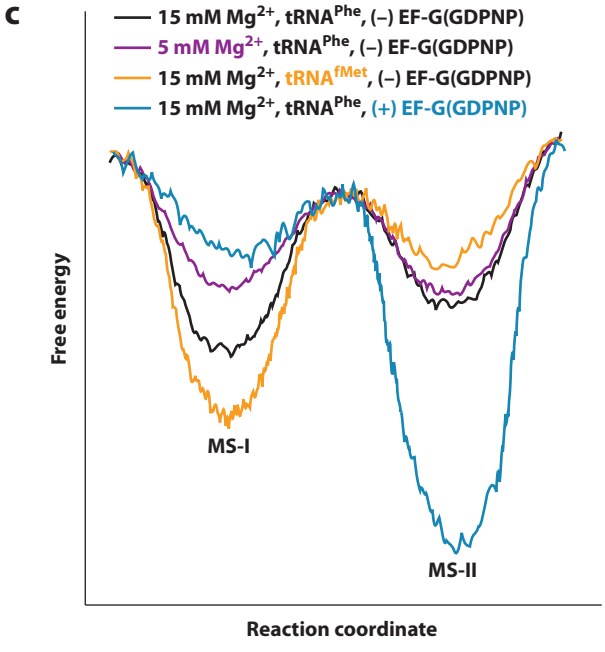

majority of smFRET studies reporting on the individual classical ⇄ hybrid tRNA (38, 58), nonrotated ⇄ rotated ribosome (43), open ⇄ closed L1 stalk (40, 42, 60), and L1◦tRNA ⇄ L1•tRNA (40, 41, 60) equilibriums within wild-type PRE complexes report fluctuations between just two major FRET states corresponding to the structures of MS-I or MS-II. Since individual MS-I ⇄ MS-II transitions must necessarily occur via some pathway (or, more likely, via any one of numerous parallel pathways), the failure of the majority of smFRET studies to detect any intermediate states connecting MS-I and MS-II is most likely due to either (*a*) the finite time resolution (typically 25–100 ms frame^{-1} in studies of ribosome dynamics) with which smFRET studies can resolve energetically unstable, and thus transiently sampled, intermediate states or (*b*) the limited spatial resolution with which a specific donor-acceptor pair signal can detect the distance change associated with formation of a particular intermediate state (even an energetically stable intermediate state). Nevertheless, emerging cryo-EM (X. Agirrezabala, H. Liao, J. Fu, J.L. Brunelle, R. Ortiz-Meoz, et al., in preparation), X-ray crystallographic (93), and smFRET (44, 52) studies have reported observations of intermediate states connecting MS-I and MS-II. We expect that the reports of these new intermediate states will drive additional structural and dynamic studies that push the structural and time resolution limits of cryo-EM, X-ray crystallography, and smFRET in an effort to elucidate the physical basis of MS-I ⇄ MS-II transitions.

3.3.2. Origin of macrostates in the ribosomal architecture. An examination of the ribosome's architecture (77, 147) reveals the origin of the rotational instability that leads to the existence of the two macrostates (37): Two massive subunits are held together by a number of bridges with varying stability depending on their location across the intersubunit plane. As a general rule, tight RNA-RNA interactions occur in the center of the ribosome particle, whereas loose interactions involving at least one ribosomal protein occur at the periphery. An example of a tight interaction is that between

Figure 5

Modulating the free-energy landscape of the macrostate (MS)-I ⇄ MS-II equilibrium. (*a*) An equilibrium single-molecule fluorescence resonance energy (smFRET) versus time trajectory for a pretranslocation (PRE) ribosomal complex sample containing a donor-labeled P-site tRNA and an acceptor-labeled L1 stalk (41), (D_5/A_5, **Figure 1*a*** and **Table 1**) (*top*). The smFRET trajectory is calculated using $I_{Cy5}/(I_{Cy3}+I_{Cy5})$, where I_{Cy3} is the raw emission intensity of the Cy3 donor fluorophore, and I_{Cy5} is the raw emission intensity of the Cy5 acceptor fluorophore. In this labeling scheme, disruption of the L1 stalk-P/E (denoting the 30S P/50S E sites, respectively) tRNA contact (L1◦tRNA, MS-I) generates a FRET value centered at 0.16 FRET, whereas formation of the L1 stalk-P/E tRNA contact (L1•tRNA, MS-II) generates a FRET value centered at 0.76 FRET. Analysis of the dwell time spent in the MS-I state prior to transitioning to the MS-II state provides the average rate constant governing MS-I → MS-II transitions, and the analogous analysis for the dwell time spent in MS-II provides the average rate constant governing MS-II → MS-I transitions. These average rate constants can be converted to free energies of activation, $\Delta G^{\ddagger}$, for the two transitions using the equation $\Delta G^{\ddagger} = -RT\ln(hk/k_BT)$, where R is the universal gas constant (8.314 J K^{-1} mol^{-1}), T is the temperature (in K), h is Planck's constant (6.626×10^{-34} J s), k is the rate constant (in s), and k_B is Boltzmann's constant (1.381×10^{-23} J K^{-1}). The smFRET trajectory shown here, used as a point of reference, was recorded using a PRE complex containing a phenylalanine-specific tRNA ($tRNA^{Phe}$) in the P site, an unoccupied A site, and no addition of elongation factor G·guanylyl iminodiphosphate (EF-G·GDPNP) in a buffer containing 15 mM Mg^{2+}. A contour plot of the time evolution of population FRET (*bottom*) is generated by superimposing the first five of numerous individual smFRET trajectories, binning the data into 20 FRET bins and 30 time bins, and normalizing the resulting data to the most populated bin in the plot. N indicates the number of trajectories used to generate the contour plot. (*b*) Inspection of the smFRET trajectories (*top*) and contour plots of the time evolution of population FRET (*bottom*) reveal that lowering the [Mg^{2+}] from 15 mM to 5 mM (*left*), replacing the P-site $tRNA^{Phe}$ with formylmethionine specific tRNA ($tRNA^{fMet}$) (*center*), and binding of EF-G·GDPNP (*right*) all markedly alter the free-energy landscape of the MS-I ⇄ MS-II equilibrium, changing the average rates and corresponding $\Delta G^{\ddagger}$s for the MS-I → MS-II and MS-II → MS-I transitions and thereby modulating the observed MS-I and MS-II equilibrium populations. (*c*) Two-dimensional free-energy profile of the MS-I ⇄ MS-II equilibrium in which the conformational space coordinate has been averaged to a single average conformer. The plot summarizes how the $\Delta G^{\ddagger}$ for the MS-I → MS-II and MS-II → MS-I transitions is altered by changes in [Mg^{2+}], P-site tRNA identity, and EF-G·GDPNP binding.

helix 44 on the 30S subunit and helix 69 on the 50S subunit (i.e., bridge B2a), and an example of a loose interaction is that between ribosomal protein S19 on the 30S subunit and helix 38 on the 50S subunit (i.e., bridge B1a).

The architectural properties of the ribosome are such that they give rise to a rotational motion when the molecule is in its thermal environment, as shown by normal mode analysis either of the X-ray structure (138, 148) or of an elastic network representation of the cryo-EM density map itself (149). These studies all indicated that intersubunit rotation is indeed a predominant mode of motion in this molecule. Normal-mode analysis also revealed a correlated motion of the L1 stalk; however, this motion goes in the opposite direction: As the 30S subunit rotates counterclockwise, the L1 stalk moves clockwise, toward the intersubunit space, again in agreement with experimental findings (40–43, 60, 62, 63, 68). Movement of the L1 stalk has been implicated in the transport of the deacylated tRNA from the P/P to the P/E position (41, 63). Thus, we have the important result that the ribosome is constructed in such a way that energy supplied from the ambient surroundings is harnessed toward productive work (99, 148).

Quite likely, this rationale of optimal energy harnessing is the reason why the intersubunit motion is encountered in other translational processes, as well (see tabulation in Reference 99).

1. In initiation, GTP hydrolysis and the release of initiation factor 2 in its GDP form from the ribosomal initiation complex are accompanied by a MS-II → MS-I transition (48, 150, 151), implying that the ribosomal initiation complex is initially assembled in MS-II, and then brought into MS-I, the proper state for acceptance of the first ternary complex of the elongation cycle.
2. In termination, the binding of GTP to ribosome-bound release factor 3 triggers an MS-I → MS-II transition of the ribosomal termination complex (57, 137, 152, 153); this conformational change is responsible for the dissociation of release factor 1 or 2 from a ribosomal termination complex (57, 153).
3. In ribosome recycling, binding of ribosome recycling factor to the posttermination ribosomal complex biases the ribosome toward MS-II (57, 154, 155).

3.3.3. Modulating the complex free-energy landscape of the MS-I ⇄ MS-II equilibrium. As expected for a complex free-energy landscape, the depths of the valleys and heights of the peaks underlying the MS-I ⇄ MS-II equilibrium are affected by a variety of factors. For example, using smFRET signals directly reporting on either the classical ⇄ hybrid tRNA, nonrotated ⇄ rotated ribosome, open ⇄ closed L1 stalk, or L1∘tRNA ⇄ L1•tRNA equilibriums as proxies for the MS-I ⇄ MS-II equilibrium, the presence of a nascent polypeptide chain versus an amino acid on the A-site tRNA decreases $\Delta G^{\ddagger}$ for the MS-I → MS-II transition by ∼4 kJ mol^{-1} while having little to no effect on $\Delta G^{\ddagger}$ for the MS-II → MS-I transition (38, 41, 44). Likewise, lowering the [Mg^{2+}] from 15 mM to 3.5 mM decreases $\Delta G^{\ddagger}$ for the MS-I → MS-II transition by ∼3 kJ mol^{-1} but has little to no effect on $\Delta G^{\ddagger}$ for the MS-II → MS-I transition (**Figure 5**) (58; J. Fei & R.L. Gonzalez, Jr., in preparation). Similarly, the identity of the P-site tRNA can modulate the free-energy landscape underlying the MS-I ⇄ MS-II equilibrium; for example, formylmethionine-specific tRNA ($tRNA^{fMet}$) increases $\Delta G^{\ddagger}$ for the MS-I → MS-II transition by ∼1 kJ mol^{-1} and decreases $\Delta G^{\ddagger}$ for the MS-II → MS-I transition by ∼2 kJ mol^{-1} relative to phenylalanine-specific tRNA ($tRNA^{Phe}$), thereby providing the mechanistic basis for the widely reported propensity of $tRNA^{fMet}$ to occupy the classical P/P configuration (40, 41), findings that have been subsequently confirmed (42, 43, 52, 53).

The ruggedness of a free-energy landscape typically speaks to the scale of the conformational change(s) that can be derived from a specified change in energy. In the case of

a smooth free-energy landscape, thermal fluctuations, which are small in energy, can yield only correspondingly small changes in structure. In contrast, thermal fluctuations within a rugged free-energy landscape can lead to large conformational changes (17). Thus, the observation that thermal fluctuations can propel the large-scale conformational changes encompassing MS-I ⇄ MS-II transitions (38, 40–44, 52–54, 58, 60, 62, 68) reveals the rugged nature of the free-energy landscape underlying the translocation reaction. The ruggedness takes into account a property of MS-I ⇄ MS-II transitions that is both predicted and more recently observed. The complexity of the structural rearrangement encompassed by MS-I ⇄ MS-II transitions, shown by atomic modeling of cryo-EM density maps for MS-I and II (68), leads us to predict that individual transitions involve an entire cascade of individual small-scale rearrangements. This suggests the existence of subsidiary minima within the valleys characterizing MS-I and MS-II, thereby yielding substates that are individually populated. Interventions, such as tRNA or ribosome mutagenesis or modification (including the fluorescent labeling necessary for smFRET studies), depletion of functionally important ribosomal proteins from ribosomes, binding of antibiotic inhibitors of translocation, replacing tRNAs with ASLs, subjecting ribosomes to crystal packing forces, et cetera, may lead to the lowering of one of the subsidiary wells and thus bias the system toward the corresponding substate. Experimental evidence for the existence of such substates is now emerging from cryo-EM (156), X-ray crystallography (93), and smFRET (44, 52). For instance, using an smFRET signal reporting on classical ⇄ hybrid tRNA transitions, the transition from the classical A/A and P/P configuration to the hybrid A/P and P/E configuration within a PRE complex containing a ribosomal RNA mutation that destabilizes the A/P configuration was proposed to significantly populate an A/A and P/E intermediate configuration (44), an intermediate configuration that had been previously proposed on the basis of tRNA mutagenesis experiments (157) and ensemble kinetic measurements (158) using wild-type PRE complexes. Indeed, a cryo-EM reconstruction of the mutant PRE complex shows that the majority of imaged particles are in an intermediate state between MS-I and MS-II (state 8, **Figure 3)** in which the tRNAs occupy the A/A and P/E configuration (156). Although the same smFRET study proposed that the A/A and P/E intermediate configuration is also significantly populated in wild-type PRE complexes, two cryo-EM studies of wild-type PRE complexes failed to observe this intermediate (62, 68). This discrepancy between the smFRET and cryo-EM studies most likely arises from the present time and/or structural resolutions with which such intermediates can be defined by either smFRET or cryo-EM in wild-type PRE complexes (29). Similarly, recent X-ray crystal structures of a new crystal form of the 70S ribosome crystallized in (*a*) the absence of tRNAs, (*b*) in the presence of a P-site tRNA ASL, and (*c*) the presence of both A- and P-site tRNA ASLs have revealed an additional intermediate state between MS-I and MS-II that can be stabilized by confinement of a wild-type ribosome within a packed crystal in the absence of intact tRNAs (93). We expect that such experiments will continue to define the rugged free-energy landscape underlying the MS-I ⇄ MS-II equilibrium.

Perhaps the largest alteration of the rugged free-energy landscape underlying the MS-I ⇄ MS-II equilibrium, and certainly the most important in terms of a Brownian motor mechanism of translocation, is the effect of EF-G·GTP binding. As described above, MS-I ⇄ MS-II transitions are stochastic and thermally driven such that MS-II is transiently sampled in the absence of EF-G·GTP, one of the hallmarks of a Brownian motor mechanism. Thus, binding of EF-G·GTP to the PRE complex should serve to rectify these stochastic MS-I ⇄ MS-II fluctuations such that MS-II is conformationally selected and/or transiently stabilized en route to the second step of the translocation reaction, namely the EF-G-catalyzed translocation of the tRNA anticodon ends and the mRNA on the 30S subunit.

Indeed, this is exactly what has been observed using multiple smFRET signals reporting on the nonrotated ⇄ rotated ribosome (43), open ⇄ closed L1 stalk (40, 42), and L1•tRNA ⇄ L1•tRNA (41, 53) equilibriums within analogs of PRE complexes in which the P site contains a deacylated tRNA and the A site is unoccupied (PRE^{-A}). In all cases, the binding of EF-G·GDPNP rectifies the system toward MS-II. Interestingly, EF-G·GDPNP-bound PRE^{-A} complexes can still exhibit spontaneous MS-I ⇄ MS-II fluctuations, indicating that such complexes are not necessarily statically trapped in MS-II (40). In fact, binding of EF-G·GDPNP to a PRE^{-A} complex can increase the frequency with which such fluctuations occur relative to that observed in the corresponding, EF-G·GDPNP-free PRE^{-A} complex. EF-G binding, therefore, can rectify MS-I ⇄ MS-II fluctuations toward MS-II either by lowering the $\Delta G^{\ddagger}$ for the MS-I → MS-II transition and/or by raising the $\Delta G^{\ddagger}$ for the MS-II → MS-I transition. Perhaps most interestingly, the identity of the P-site tRNA dictates the kinetic strategy used by EF-G. For example, in the presence of P site–bound $tRNA^{fMet}$, EF-G lowers $\Delta G^{\ddagger}$ for the MS-I → MS-II transition by ∼5 kJ mol^{-1} while having little to no effect on $\Delta G^{\ddagger}$ for the MS-II → MS-I transition. Contrasting with this result, the presence of a P site–bound $tRNA^{Phe}$ raises $\Delta G^{\ddagger}$ for the MS-II → MS-I transition so high that this transition becomes virtually inaccessible, effectively trapping the system in MS-II. Satisfyingly, the dynamic nature of the EF-G·GDPNP-bound PRE^{-A} complex and the P-site tRNA-dependent regulation of these dynamics have been recently confirmed (53). It is particularly remarkable that the direct binding interactions that EF-G·GDPNP makes with the ribosome at the factor-binding site near the A site can allosterically modulate the kinetics of L1 stalk opening and closing at a hinge that is located ∼170 Å away within the E site; this observation highlights the long-range allosteric coupling that links the various dynamic processes that operate within the PRE complex (40).

3.3.4. A Brownian motor mechanism may also underlie translocation of the tRNA anticodons and the mRNA on the 30S subunit. The observation that, in the absence of EF-G, the ribosome can efficiently reverse-translocate the entire tRNA-mRNA complex under certain experimental conditions (159, 160) strongly supports the hypothesis that Brownian motor mechanisms underlie the entire translocation reaction. Thus, in addition to the Brownian motor mechanism that drives translocation of the tRNA acceptor ends within the 50S subunit, a Brownian motor mechanism might also underlie translocation of the tRNA anticodons and the mRNA on the 30S subunit. In this scenario, binding of EF-G·GTP would rectify MS-I ⇄ MS-II fluctuations toward MS-II, and upon ribosome-stimulated GTP hydrolysis, EF-G·GDP would serve to rectify fluctuations of the tRNA anticodons and the mRNA in the forward direction (i.e., toward POST-2 in **Figure 4**). Indeed, LepA (EF-4), a recently discovered translational GTPase that catalyzes reverse translocation (161), may have the opposite function, namely to rectify fluctuations of the tRNA anticodons and the mRNA in the reverse direction (i.e., toward POST-1 in **Figure 4**). The use of smFRET studies to investigate reverse translocation and the roles of EF-G and LepA in promoting forward and reverse translocation, respectively, should provide the means for testing these possibilities.

4. FUTURE GOALS AND PERSPECTIVES

The current driving forces in the characterization of ribosomal dynamics and the way they affect translation are cryo-EM, X-ray crystallography, and smFRET. The emerging view of the ribosome as a processive Brownian motor, whose states are described by a rugged free-energy landscape that can be modulated by environmental conditions as well as by the ribosome's tRNA substrates and accessory translation factors, makes it clear how little we know from experiments to date. It is even more humbling to realize that the free-energy

landscape describing elongation that is used as an example in **Figure 4** is just one of numerous such landscapes that will require detailed study. For example, the scope of this article has not allowed us to discuss further modifications of the elongation free-energy landscape by the interactions that the exiting polypeptide makes with the ribosomal exit tunnel as well as with the translocon, which are clearly required to round up the characterization of states. Beyond elongation, the initiation, termination, and ribosome recycling stages of protein synthesis all also involve an MS-I → MS-II transition (99, 150–155). Indeed, very recent smFRET studies have demonstrated how initiation factors (48), release factors (57), and ribosome recycling factors (57) rectify and thereby regulate the MS-I ⇄ MS-II equilibrium during the initiation, termination, and ribosome recycling stages of protein synthesis. A true understanding of the workings of the ribosome as a molecular motor will require a continued effort to sample the relevant landscapes systematically, covering all important substates and macrostates by cryo-EM or, when feasible, by X-ray crystallography, and all transitions among these substates and macrostates by smFRET.

Efforts to reach this goal still face a number of obstacles. Resolving the substates by cryo-EM with the necessary spatial resolution requires a substantial increase in data collection and a sharpening of classification tools. The prospect of digital online data capture with 8000 × 8000 pixel field size on the electron microscope becoming an affordable option offers hope that data collection in the millions of particles will be a reality. Regarding classification, the recent works by the Carazo (162, 163) and Penczek (164, 165) groups have given us valuable tools for unsupervised classification, i.e., without the need to use reference structures. Exciting progress is also being made in the development of time-resolved electron microscopy through the employment of flash photolysis or nanotechnology (166, 167). Thanks to these efforts, it is now possible to obtain a two-component mix of ribosome and substrate (such as EF-G) at a defined time point and freeze the mixture at some point several milliseconds later (167). By changing the length of reaction time in a systematic way, it should be possible to follow the emergence of newly occupied states.

Likewise, several limitations currently restrict the potential of smFRET, defining areas that would benefit from further technical development. Perhaps the major limitation involves the ever-present trade-offs between time resolution, signal-to-noise ratio, and the efficiency with which large, statistically relevant data sets can be collected. On the one hand, wide-field microscopies, such as total internal reflection fluorescence microscopy, allow data to be simultaneously collected on hundreds of molecules with a time resolution on the order of tens of milliseconds to hundreds of milliseconds (95, 168), limited primarily by the signal-to-noise ratio of the data but also by the ability of the computer to rapidly write the data to disk. Although these techniques allow a large, statistically relevant data set to be collected relatively rapidly, the time resolution may not be high enough to characterize short-lived, but mechanistically interesting, conformational substates. On the other hand, confocal fluorescence microscopies allow data to be collected on one molecule at a time with microseconds to tens of microseconds time resolution (95, 168). Here the time resolution promises data that will be mechanistically richer but will require longer periods of data collection to generate large, statistically relevant data sets. Finally, model-free inference of the number of states underlying smFRET versus time trajectories and the corresponding rates of transitions between these states remains a major goal of developing data analysis algorithms. Currently, most data analysis methods model the observed smFRET trajectories using a hidden Markov model and implement a maximum likelihood-based inference approach on individual trajectories that requires the user to either guess the number of states present in the data or overfit the data intentionally by asserting an excess number of states (169–172). Recently, however, a variational Bayesian approach has been introduced that allows inference of the number of states

and transition rates between states from individual smFRET trajectories without requiring user guesses and/or overfitting (40, 60).

The fact that cryo-EM and smFRET can draw complementary pictures of the same process provides great opportunities in coming to an understanding of translation. However, future studies aiming to integrate data from cryo-EM with those of smFRET in a more quantitative way will require looking at the same sample with both techniques because there are many indications that even small changes in experimental conditions and molecular constructs may have pronounced effects on the free-energy landscape.

SUMMARY POINTS

1. The ribosome is a highly dynamic molecular machine, specifically a processive Brownian motor.
2. The conformational dynamics of the ribosome, and the way the ribosome interacts with its ligands, have been experimentally studied by three primary methods: cryo-EM and X-ray crystallography, yielding three-dimensional snapshots, and, more recently, smFRET, yielding the real-time conformational trajectories of single molecules.
3. Detailed insights into the molecular mechanisms underlying aa-tRNA selection and mRNA-tRNA translocation can be gained by combining results from cryo-EM, X-ray crystallography, and smFRET.
4. smFRET studies indicate that, during both aa-tRNA selection and translocation, ribosomes and tRNAs fluctuate among several conformational states and that the choices of pathways taken are sensitive to many factors, such as the exact experimental conditions, the identity of the tRNAs involved, the presence of small-molecule antibiotic inhibitors of aa-tRNA selection and/or translocation, and the action of translation factors.
5. Translocation is facilitated by architectural features of the ribosome that allow it to interconvert between two conformations, or macrostates, with little expenditure of energy. These states are linked to the transition of the tRNA configuration from classical A/A and P/P configurations to the hybrid A/P and P/E configurations.
6. Evidence from smFRET and cryo-EM for spontaneous transitions between the macrostates has led to a revision of the role of EF-G in translocation, from instrumental to ancillary, accelerating a process structurally ingrained in the ribosome.
7. A free-energy landscape depiction of the degrees of freedom of the complex formed by ribosome and its ligands during the elongation cycle is a useful heuristic tool, which suggests that concepts recently developed in the study of enzyme catalysis are applicable to this much larger system.

FUTURE ISSUES

1. In terms of the free-energy landscape of translation, our current knowledge is restricted predominantly to elongation and is limited to only a few states and pathways. A detailed, systematic mapping of the full landscape throughout all stages of protein synthesis is clearly required.

2. As far as cryo-EM is concerned, addressing this broad program will require two developments: (*a*) time-resolved methods allowing the study of a presteady-state system developing over time and (*b*) further advances in classification methods to sort heterogeneous molecular populations into homogeneous subsets.
3. Likewise, the use of smFRET for mapping out the free-energy landscapes of the translating ribosome will benefit greatly from several developments: (*a*) further advances in detector technologies to increase the signal-to-noise ratio and time resolution, (*b*) automated and high-throughput data collection schemes to improve the efficiency with which large, statistically relevant data sets can be collected, and (*c*) continued development of automated, high-throughput, and model-free data analysis algorithms.
4. As the experimental knowledge base on ribosomal dynamics from cryo-EM, X-ray crystallography, and smFRET increases, molecular dynamics simulations of selected pathways will lead to a fuller understanding of molecular mechanisms of translation.

DISCLOSURE STATEMENT

The authors are not aware of any affiliations, memberships, funding, or financial holdings that might be perceived as affecting the objectivity of this review.

ACKNOWLEDGMENTS

This work was supported by HHMI and NIH-NIGMS grants (R37 GM29169 and R01 GM55440) to J.F. and a Burroughs Wellcome Fund CABS Award (CABS 1004856), an NSF CAREER Award (MCB 0644262), an NIH-NIGMS grant (R01 GM084288), and an American Cancer Society Research Scholar Grant (RSG GMC-117152) to R.L.G. We thank Jingyi Fei, Daniel D. MacDougall, Joseph D. Puglisi, Colin E. Aitken, and Peter V. Cornish for insightful discussions, Li Wen, Bo Chen, Jingyi Fei, Daniel D. MacDougall, and Margaret M. Elvekrog for comments on the manuscript, and Lila Iino-Rubenstein, Jingyi Fei, and Jonathan E. Bronson for assistance with the preparation of the illustrations.

LITERATURE CITED

1. Spirin AS. 2002. Ribosome as a molecular machine. *FEBS Lett.* 514:2–10
2. Garai A, Chowdhury D, Ramakrishnan TV. 2009. Stochastic kinetics of ribosomes: single motor properties and collective behavior. *Phys. Rev. E.* 80:011908
3. Spirin AS. 2009. The ribosome as a conveying thermal ratchet machine. *J. Biol. Chem.* 284:21103–19
4. Spirin AS. 2004. The ribosome as an RNA-based molecular machine. *RNA Biol.* 1:3–9
5. Astumian RD. 1997. Thermodynamics and kinetics of a Brownian motor. *Science* 276:917–22
6. Peskin CS, Odell GM, Oster GF, Cordova NJ, Ermentrout B. 1993. Cellular motions and thermal fluctuations: the Brownian ratchet. *Biophys. J.* 65:316–24
7. Cordova NJ, Ermentrout B, Oster GF. 1992. Dynamics of single-motor molecules: the thermal ratchet model. *Proc. Natl. Acad. Sci. USA* 89:339–43
8. Abbondanzieri EA, Greenleaf WJ, Shaevitz JW, Landick R, Block SM. 2005. Direct observation of base-pair stepping by RNA polymerase. *Nature* 438:460–65
9. Bai L, Shundrovsky A, Wang MD. 2004. Sequence-dependent kinetic model for transcription elongation by RNA polymerase. *J. Mol. Biol.* 344:335–49
10. Bryngelson JD, Onuchic JN, Socci ND, Wolynes PG. 1995. Funnels, pathways, and the energy landscape of protein folding: a synthesis. *Proteins* 21:167–95

11. Onuchic JN, Wolynes PG. 2004. Theory of protein folding. *Curr. Opin. Struct. Biol.* 14:70–75
12. Shcherbakova I, Mitra S, Laederach A, Brenowitz M. 2008. Energy barriers, pathways, and dynamics during folding of large, multidomain RNAs. *Curr. Opin. Chem. Biol.* 12:655–66
13. Thirumalai D, Lee N, Woodson SA, Klimov D. 2001. Early events in RNA folding. *Annu. Rev. Phys. Chem.* 52:751–62
14. Bokinsky G, Zhuang XW. 2005. Single-molecule RNA folding. *Acc. Chem. Res.* 38:566–73
15. Chu VB, Herschlag D. 2008. Unwinding RNA's secrets: advances in the biology, physics, and modeling of complex RNAs. *Curr. Opin. Struct. Biol.* 18:305–14
16. Treiber DK, Williamson JR. 2001. Beyond kinetic traps in RNA folding. *Curr. Opin. Struct. Biol.* 11:309–14
17. Dill KA, Chan HS. 1997. From Levinthal to pathways to funnels. *Nat. Struct. Biol.* 4:10–19
18. Schnell JR, Dyson HJ, Wright PE. 2004. Structure, dynamics, and catalytic function of dihydrofolate reductase. *Annu. Rev. Biophys. Biomol. Struct.* 33:119–40
19. Zhuang X, Kim H, Pereira MJ, Babcock HP, Walter NG, Chu S. 2002. Correlating structural dynamics and function in single ribozyme molecules. *Science* 296:1473–76
20. Nagel ZD, Klinman JP. 2006. Tunneling and dynamics in enzymatic hydride transfer. *Chem. Rev.* 106:3095–118
21. Benkovic SJ, Hammes GG, Hammes-Schiffer S. 2008. Free-energy landscape of enzyme catalysis. *Biochemistry* 47:3317–21
22. Hammes-Schiffer S, Benkovic SJ. 2006. Relating protein motion to catalysis. *Annu. Rev. Biochem.* 75:519–41
23. Cole R, Loria JP. 2002. Evidence for flexibility in the function of ribonuclease A. *Biochemistry* 41:6072–81
24. Das K, Bauman JD, Clark AD Jr, Frenkel YV, Lewi PJ, et al. 2008. High-resolution structures of HIV-1 reverse transcriptase/TMC278 complexes: Strategic flexibility explains potency against resistance mutations. *Proc. Natl. Acad. Sci. USA* 105:1466–71
25. Zhuang XW. 2005. Single-molecule RNA science. *Annu. Rev. Biophys. Biomol. Struct.* 34:399–414
26. Zhuang X, Bartley LE, Babcock HP, Russell R, Ha T, et al. 2000. A single-molecule study of RNA catalysis and folding. *Science* 288:2048–51
27. English BP, Min W, van Oijen AM, Lee KT, Luo G, et al. 2006. Ever-fluctuating single enzyme molecules: Michaelis-Menten equation revisited. *Nat. Chem. Biol.* 2:87–94
28. Boehr DD, McElheny D, Dyson HJ, Wright PE. 2006. The dynamic energy landscape of dihydrofolate reductase catalysis. *Science* 313:1638–42
29. Munro JB, Sanbonmatsu KY, Spahn CM, Blanchard SC. 2009. Navigating the ribosome's metastable energy landscape. *Trends Biochem. Sci.* 34:390–400
30. Frank J, Agrawal RK. 2000. A ratchet-like inter-subunit reorganization of the ribosome during translocation. *Nature* 406:318–22
31. Korostelev A, Ermolenko DN, Noller HF. 2008. Structural dynamics of the ribosome. *Curr. Opin. Chem. Biol.* 12:674–83
32. Koshland DE Jr. 1958. Application of a theory of enzyme specificity to protein synthesis. *Proc. Natl. Acad. Sci. USA* 44:98–104
33. Williamson JR. 2000. Induced fit in RNA-protein recognition. *Nat. Struct. Biol.* 7:834–37
34. Tsai CJ, Kumar S, Ma B, Nussinov R. 1999. Folding funnels, binding funnels, and protein function. *Protein Sci.* 8:1181–90
35. Bosshard HR. 2001. Molecular recognition by induced fit: How fit is the concept? *News Physiol. Sci.* 16:171–73
36. Wang C, Karpowich N, Hunt JF, Rance M, Palmer AG. 2004. Dynamics of ATP-binding cassette contribute to allosteric control, nucleotide binding and energy transduction in ABC transporters. *J. Mol. Biol.* 342:525–37
37. Wen JD, Lancaster L, Hodges C, Zeri AC, Yoshimura SH, et al. 2008. Following translation by single ribosomes one codon at a time. *Nature* 452:598–603
38. Blanchard SC, Kim HD, Gonzalez RL Jr, Puglisi JD, Chu S. 2004. tRNA dynamics on the ribosome during translation. *Proc. Natl. Acad. Sci. USA* 101:12893–98

39. Blanchard SC, Gonzalez RL Jr, Kim HD, Chu S, Puglisi JD. 2004. tRNA selection and kinetic proofreading in translation. *Nat. Struct. Mol. Biol.* 11:1008–14
40. Fei J, Bronson JE, Hofman JM, Srinivas RL, Wiggins CH, Gonzalez RLJ. 2009. Allosteric collaboration between elongation factor G and the ribosomal L1 stalk directs tRNA movements during translation. *Proc. Natl. Acad. Sci. USA* 106:15702–7
41. Fei J, Kosuri P, MacDougall DD, Gonzalez RL Jr. 2008. Coupling of ribosomal L1 stalk and tRNA dynamics during translation elongation. *Mol. Cell* 30:348–59
42. Cornish PV, Ermolenko DN, Staple DW, Hoang L, Hickerson RP, et al. 2009. Following movement of the L1 stalk between three functional states in single ribosomes. *Proc. Natl. Acad. Sci. USA* 106:2571–76
43. Cornish PV, Ermolenko DN, Noller HF, Ha T. 2008. Spontaneous intersubunit rotation in single ribosomes. *Mol. Cell* 30:578–88
44. Munro JB, Altman RB, O'Connor N, Blanchard SC. 2007. Identification of two distinct hybrid state intermediates on the ribosome. *Mol. Cell* 25:505–17
45. Marshall RA, Dorywalska M, Puglisi JD. 2008. Irreversible chemical steps control intersubunit dynamics during translation. *Proc. Natl. Acad. Sci. USA* 105:15364–69
46. Wang Y, Qin H, Kudaravalli RD, Kirillov SV, Dempsey GT, et al. 2007. Single-molecule structural dynamics of EF-G–ribosome interaction during translocation. *Biochemistry* 46:10767–75
47. Uemura S, Dorywalska M, Lee TH, Kim HD, Puglisi JD, Chu S. 2007. Peptide bond formation destabilizes Shine-Dalgarno interaction on the ribosome. *Nature* 446:454–57
48. Marshall RA, Aitken CE, Puglisi JD. 2009. GTP hydrolysis by IF2 guides progression of the ribosome into elongation. *Mol. Cell* 35:37–47
49. Vanzi F, Vladimirov S, Knudsen CR, Goldman YE, Cooperman BS. 2003. Protein synthesis by single ribosomes. *RNA* 9:1174–79
50. Vanzi F, Takagi Y, Shuman H, Cooperman BS, Goldman YE. 2005. Mechanical studies of single ribosome/mRNA complexes. *Biophys. J.* 89:1909–19
51. Dorywalska M, Blanchard SC, Gonzalez RL, Kim HD, Chu S, Puglisi JD. 2005. Site-specific labeling of the ribosome for single-molecule spectroscopy. *Nucleic Acids Res.* 33:182–89
52. Munro JB, Altman RB, Tung CS, Cate JH, Sanbonmatsu KY, Blanchard SC. 2010. Spontaneous formation of the unlocked state of the ribosome is a multistep process. *Proc. Natl. Acad. Sci. USA.* 107:709–14
53. Munro JB, Altman RB, Tung CS, Sanbonmatsu KY, Blanchard SC. 2010. A fast dynamic mode of the EF-G-bound ribosome. *EMBO J.* 29:770–81
54. Feldman MB, Terry DS, Altman RB, Blanchard SC. 2009. Aminoglycoside activity observed on single pre-translocation ribosome complexes. *Nat. Chem. Biol.* 6:54–62
55. Effraim PR, Wang J, Englander MT, Avins J, Leyh TS, et al. 2009. Natural amino acids do not require their native tRNAs for efficient selection by the ribosome. *Nat. Chem. Biol.* 5:947–53
56. Gonzalez RL Jr, Chu S, Puglisi JD. 2007. Thiostrepton inhibition of tRNA delivery to the ribosome. *RNA* 13:2091–97
57. Sternberg SH, Fei J, Prywes N, McGrath KA, Gonzalez RL Jr. 2009. Translation factors direct intrinsic ribosome dynamics during translation termination and ribosome recycling. *Nat. Struct. Mol. Biol.* 16:861–68
58. Kim HD, Puglisi J, Chu S. 2007. Fluctuations of transfer RNAs between classical and hybrid states. *Biophys. J.* 93:3575–82
59. Lee TH, Blanchard SC, Kim HD, Puglisi JD, Chu S. 2007. The role of fluctuations in tRNA selection by the ribosome. *Proc. Natl. Acad. Sci. USA* 104:13661–65
60. Bronson JE, Fei J, Hofman JM, Gonzalez RL Jr, Wiggins CH. 2009. Learning rates and states from biophysical time series: a Bayesian approach to model selection and single-molecule FRET data. *Biophys. J.* 97:3196–205
61. Villa E, Sengupta J, Trabuco LG, LeBarron J, Baxter WT, et al. 2009. Ribosome-induced changes in elongation factor Tu conformation control GTP hydrolysis. *Proc. Natl. Acad. Sci. USA* 106:1063–68
62. Julian P, Konevega AL, Scheres SH, Lazaro M, Gil D, et al. 2008. Structure of ratcheted ribosomes with tRNAs in hybrid states. *Proc. Natl. Acad. Sci. USA* 105:16924–27
63. Valle M, Zavialov AV, Sengupta J, Rawat U, Ehrenberg M, Frank J. 2003. Locking and unlocking of ribosomal motions. *Cell* 114:123–34

64. Valle M, Zavialov A, Li W, Stagg SM, Sengupta J, et al. 2003. Incorporation of aminoacyl-tRNA into the ribosome as seen by cryo-electron microscopy. *Nat. Struct. Biol.* 10:899–906
65. Li W, Agirrezabala X, Lei J, Bouakaz L, Brunelle JL, et al. 2008. Recognition of aminoacyl-tRNA: a common molecular mechanism revealed by cryo-EM. *EMBO J.* 27:3322–31
66. Stark H, Rodnina MV, Wieden HJ, Zemlin F, Wintermeyer W, van Heel M. 2002. Ribosome interactions of aminoacyl-tRNA and elongation factor Tu in the codon-recognition complex. *Nat. Struct. Biol.* 9:849–54
67. Stark H, Rodnina MV, Wieden HJ, van Heel M, Wintermeyer W. 2000. Large-scale movement of elongation factor G and extensive conformational change of the ribosome during translocation. *Cell* 100:301–9
68. Agirrezabala X, Lei J, Brunelle JL, Ortiz-Meoz RF, Green R, Frank J. 2008. Visualization of the hybrid state of tRNA binding promoted by spontaneous ratcheting of the ribosome. *Mol. Cell* 32:190–97
69. Schuette JC, Murphy FV 4th, Kelley AC, Weir JR, Giesebrecht J, et al. 2009. GTPase activation of elongation factor EF-Tu by the ribosome during decoding. *EMBO J.* 28:755–65
70. Schmeing TM, Seila AC, Hansen JL, Freeborn B, Soukup JK, et al. 2002. A pre-translocational intermediate in protein synthesis observed in crystals of enzymatically active 50S subunits. *Nat. Struct. Biol.* 9:225–30
71. Korostelev A, Trakhanov S, Laurberg M, Noller HF. 2006. Crystal structure of a 70S ribosome-tRNA complex reveals functional interactions and rearrangements. *Cell* 126:1065–77
72. Selmer M, Dunham CM, Murphy FV 4th, Weixlbaumer A, Petry S, et al. 2006. Structure of the 70S ribosome complexed with mRNA and tRNA. *Science* 313:1935–42
73. Ogle JM, Murphy FV, Tarry MJ, Ramakrishnan V. 2002. Selection of tRNA by the ribosome requires a transition from an open to a closed form. *Cell* 111:721–32
74. Ogle JM, Brodersen DE, Clemons WM Jr, Tarry MJ, Carter AP, Ramakrishnan V. 2001. Recognition of cognate transfer RNA by the 30S ribosomal subunit. *Science* 292:897–902
75. Carter AP, Clemons WM, Brodersen DE, Morgan-Warren RJ, Wimberly BT, Ramakrishnan V. 2000. Functional insights from the structure of the 30S ribosomal subunit and its interactions with antibiotics (see comments). *Nature* 407:340–48
76. Wimberly BT, Brodersen DE, Clemons WM Jr, Morgan-Warren RJ, Carter AP, et al. 2000. Structure of the 30S ribosomal subunit. *Nature* 407:327–39 (also comment pp. 306–7)
77. Yusupov MM, Yusupova GZ, Baucom A, Lieberman K, Earnest TN, et al. 2001. Crystal structure of the ribosome at 5.5 A resolution. *Science* 292:883–96
78. Yusupova GZ, Yusupov MM, Cate JH, Noller HF. 2001. The path of messenger RNA through the ribosome. *Cell* 106:233–41
79. Cate JH, Yusupov MM, Yusupova GZ, Earnest TN, Noller HF. 1999. X-ray crystal structures of 70S ribosome functional complexes. *Science* 285:2095–104
80. Schmeing TM, Moore PB, Steitz TA. 2003. Structures of deacylated tRNA mimics bound to the E site of the large ribosomal subunit. *RNA* 9:1345–52
81. Ban N, Nissen P, Hansen J, Moore PB, Steitz TA. 2000. The complete atomic structure of the large ribosomal subunit at 2.4 A resolution. *Science* 289:905–20
82. Nissen P, Hansen J, Ban N, Moore PB, Steitz TA. 2000. The structural basis of ribosome activity in peptide bond synthesis. *Science* 289:920–30
83. Harms J, Schluenzen F, Zarivach R, Bashan A, Gat S, et al. 2001. High resolution structure of the large ribosomal subunit from a mesophilic eubacterium. *Cell* 107:679–88
84. Schluenzen F, Tocilj A, Zarivach R, Harms J, Gluehmann M, et al. 2000. Structure of functionally activated small ribosomal subunit at 3.3 angstroms resolution. *Cell* 102:615–23
85. Schmeing TM, Voorhees RM, Kelley AC, Gao YG, Murphy FV 4th, et al. 2009. The crystal structure of the ribosome bound to EF-Tu and aminoacyl-tRNA. *Science* 326:688–94
86. Gao YG, Selmer M, Dunham CM, Weixlbaumer A, Kelley AC, Ramakrishnan V. 2009. The structure of the ribosome with elongation factor G trapped in the posttranslocational state. *Science* 326:694–99
87. Frank J. 2006. *Three-Dimensional Electron Microscopy of Macromolecular Assemblies*. New York: Oxford Univ. Press

88. Glaeser R, Downing K, DeRosier D, Chiu W, Frank J. 2007. *Electron Crystallography of Biological Macromolecules*. New York: Oxford Univ. Press
89. Mitra K, Frank J. 2006. Ribosome dynamics: insights from atomic structure modeling into cryo-electron microscopy maps. *Annu. Rev. Biophys. Biomol. Struct.* 35:299–317
90. Trabuco LG, Villa E, Mitra K, Frank J, Schulten K. 2008. Flexible fitting of atomic structures into electron microscopy maps using molecular dynamics. *Structure* 16:673–83
91. Schuwirth BS, Borovinskaya MA, Hau CW, Zhang W, Vila-Sanjurjo A, et al. 2005. Structures of the bacterial ribosome at 3.5 A resolution. *Science* 310:827–34
92. Carter AP, Clemons WM Jr, Brodersen DE, Morgan-Warren RJ, Hartsch T, et al. 2001. Crystal structure of an initiation factor bound to the 30S ribosomal subunit. *Science* 291:498–501
93. Zhang W, Dunkle JA, Cate JH. 2009. Structures of the ribosome in intermediate states of ratcheting. *Science* 325:1014–17
94. Ha T. 2001. Single-molecule fluorescence resonance energy. *Methods* 25:78–86
95. Joo C, Balci H, Ishitsuka Y, Buranachai C, Ha T. 2008. Advances in single-molecule fluorescence methods for molecular biology. *Annu. Rev. Biochem.* 77:51–76
96. Clamme JP, Deniz AA. 2005. Three-color single-molecule fluorescence resonance energy transfer. *ChemPhysChem* 6:74–77
97. Hohng S, Joo C, Ha T. 2004. Single-molecule three-color FRET. *Biophys. J.* 87:1328–37
98. Clegg RM. 1992. Fluorescence resonance energy transfer and nucleic acids. *Methods Enzymol.* 211:353–88
99. Frank J, Gao H, Sengupta J, Gao N, Taylor DJ. 2007. The process of mRNA-tRNA translocation. *Proc. Natl. Acad. Sci. USA* 104:19671–78
100. Taylor DJ, Nilsson J, Merrill AR, Andersen GR, Nissen P, Frank J. 2007. Structures of modified eEF2 80S ribosome complexes reveal the role of GTP hydrolysis in translocation. *EMBO J.* 26:2421–31
101. Rodnina MV, Gromadski KB, Kothe U, Wieden HJ. 2005. Recognition and selection of tRNA in translation. *FEBS Lett.* 579:938–42
102. Beringer M, Rodnina MV. 2007. The ribosomal peptidyl transferase. *Mol. Cell* 26:311–21
103. Shoji S, Walker SE, Fredrick K. 2009. Ribosomal translocation: one step closer to the molecular mechanism. *ACS Chem. Biol.* 4:93–107
104. Daviter T, Gromadski KB, Rodnina MV. 2006. The ribosome's response to codon-anticodon mismatches. *Biochimie* 88:1001–11
105. Hopfield JJ. 1974. Kinetic proofreading: a new mechanism for reducing errors in biosynthetic processes requiring high specificity. *Proc. Natl. Acad. Sci. USA* 71:4135–39
106. Rodnina MV, Wintermeyer W. 2001. Ribosome fidelity: tRNA discrimination, proofreading and induced fit. *Trends Biochem. Sci.* 26:124–30
107. Zaher HS, Green R. 2009. Fidelity at the molecular level: lessons from protein synthesis. *Cell* 136:746–62
108. Fourmy D, Recht MI, Blanchard SC, Puglisi JD. 1996. Structure of the A site of *E. coli* 16S ribosomal RNA complexed with an aminoglycoside antibiotic. *Science* 274:1367–71
109. Fourmy D, Yoshizawa S, Puglisi JD. 1998. Paromomycin binding induces a local conformational change in the A site of 16S rRNA. *J. Mol. Biol.* 277:333–45
110. Gromadski KB, Rodnina MV. 2004. Kinetic determinants of high-fidelity tRNA discrimination on the ribosome. *Mol. Cell* 13:191–200
111. Gromadski KB, Daviter T, Rodnina MV. 2006. A uniform response to mismatches in codon-anticodon complexes ensures ribosomal fidelity. *Mol. Cell* 21:369–77
112. Thomas LK, Dix DB, Thompson RC. 1988. Codon choice and gene expression: Synonymous codons differ in their ability to direct aminoacylated-transfer RNA binding to ribosomes in vitro. *Proc. Natl. Acad. Sci. USA* 85:4242–46
113. Dix DB, Thompson RC. 1989. Codon choice and gene expression: Synonymous codons differ in translational accuracy. *Proc. Natl. Acad. Sci. USA* 86:6888–92
114. Wolf H, Chinali G, Parmeggiani A. 1977. Mechanism of the inhibition of protein synthesis by kirromycin. *Eur. J. Biochem.* 75:67–75
115. Parmeggiani A, Swart GW. 1985. Mechanism of action of kirromycin-like antibiotics. *Annu. Rev. Microbiol.* 39:557–77

116. Stark H, Rodnina MV, Rinke-Appel J, Brimacombe R, Wintermeyer W, van Heel M. 1997. Visualization of elongation factor Tu on the *Escherichia coli* ribosome. *Nature* 389:403–6
117. Valle M, Sengupta J, Swami NK, Grassucci RA, Burkhardt N, et al. 2002. Cryo-EM reveals an active role for aminoacyl-tRNA in the accommodation process. *EMBO J.* 21:3557–67
118. LeBarron J, Grassucci RA, Shaikh TR, Baxter WT, Sengupta J, Frank J. 2008. Exploration of parameters in cryo-EM leading to an improved density map of the *E. coli* ribosome. *J. Struct. Biol.* 164:24–32
119. Frank J, Sengupta J, Gao H, Li W, Valle M, et al. 2005. The role of tRNA as a molecular spring in decoding, accommodation, and peptidyl transfer. *FEBS Lett.* 579:959–62
120. Shi H, Moore PB. 2000. The crystal structure of yeast phenylalanine tRNA at 1.93 A resolution: a classic structure revisited. *RNA* 6:1091–105
121. Piepenburg O, Pape T, Pleiss JA, Wintermeyer W, Uhlenbeck OC, Rodnina MV. 2000. Intact aminoacyl-tRNA is required to trigger GTP hydrolysis by elongation factor Tu on the ribosome. *Biochemistry* 39:1734–38
122. Cochella L, Green R. 2005. An active role for tRNA in decoding beyond codon:anticodon pairing. *Science* 308:1178–80
123. Ledoux S, Olejniczak M, Uhlenbeck OC. 2009. A sequence element that tunes *Escherichia coli* $tRNA_{GGC}^{Ala}$ to ensure accurate decoding. *Nat. Struct. Mol. Biol.* 16:359–64
124. Murakami H, Ohta A, Suga H. 2009. Bases in the anticodon loop of $tRNA^{Ala}_{GGC}$ prevent misreading. *Nat. Struct. Mol. Biol.* 16:353–58
125. Yarus M, Valle M, Frank J. 2003. A twisted tRNA intermediate sets the threshold for decoding. *RNA* 9:384–85
126. Brunelle JL, Youngman EM, Sharma D, Green R. 2006. The interaction between C75 of tRNA and the A loop of the ribosome stimulates peptidyl transferase activity. *RNA* 12:33–39
127. Weinger JS, Parnell KM, Dorner S, Green R, Strobel SA. 2004. Substrate-assisted catalysis of peptide bond formation by the ribosome. *Nat. Struct. Mol. Biol.* 11:1101–6
128. Youngman EM, Brunelle JL, Kochaniak AB, Green R. 2004. The active site of the ribosome is composed of two layers of conserved nucleotides with distinct roles in peptide bond formation and peptide release. *Cell* 117:589–99
129. Voorhees RM, Weixlbaumer A, Loakes D, Kelley AC, Ramakrishnan V. 2009. Insights into substrate stabilization from snapshots of the peptidyl transferase center of the intact 70S ribosome. *Nat. Struct. Mol. Biol.* 16:528–33
130. Agrawal RK, Penczek P, Grassucci RA, Frank J. 1998. Visualization of elongation factor G on the *Escherichia coli* 70S ribosome: the mechanism of translocation. *Proc. Natl. Acad. Sci. USA* 95:6134–38
131. Agrawal RK, Heagle AB, Penczek P, Grassucci RA, Frank J. 1999. EF-G-dependent GTP hydrolysis induces translocation accompanied by large conformational changes in the 70S ribosome. *Nat. Struct. Biol.* 6:643–47
132. Bretscher MS. 1968. Translocation in protein synthesis: a hybrid structure model. *Nature* 218:675–77
133. Spirin AS. 1969. A model of the functioning ribosome: locking and unlocking of the ribosome subparticles. *Cold Spring Harb. Symp. Quant. Biol.* 34:197–207
134. Moazed D, Noller HF. 1989. Intermediate states in the movement of transfer RNA in the ribosome. *Nature* 342:142–48
135. Odom OW, Picking WD, Hardesty B. 1990. Movement of tRNA but not the nascent peptide during peptide bond formation on ribosomes. *Biochemistry* 29:10734–44
136. Ermolenko DN, Spiegel PC, Majumdar ZK, Hickerson RP, Clegg RM, Noller HF. 2007. The antibiotic viomycin traps the ribosome in an intermediate state of translocation. *Nat. Struct. Mol. Biol.* 14:493–97
137. Ermolenko DN, Majumdar ZK, Hickerson RP, Spiegel PC, Clegg RM, Noller HF. 2007. Observation of intersubunit movement of the ribosome in solution using FRET. *J. Mol. Biol.* 370:530–40
138. Wang Y, Rader AJ, Bahar I, Jernigan RL. 2004. Global ribosome motions revealed with elastic network model. *J. Struct. Biol.* 147:302–14
139. Berk V, Zhang W, Pai RD, Cate JH. 2006. Structural basis for mRNA and tRNA positioning on the ribosome. *Proc. Natl. Acad. Sci. USA* 103:15830–34
140. Connell SR, Takemoto C, Wilson DN, Wang H, Murayama K, et al. 2007. Structural basis for interaction of the ribosome with the switch regions of GTP-bound elongation factors. *Mol. Cell* 25:751–64

141. Tama F, Miyashita O, Brooks CL 3rd. 2004. Normal mode based flexible fitting of high-resolution structure into low-resolution experimental data from cryo-EM. *J. Struct. Biol.* 147:315–26
142. Blaha G, Stanley RE, Steitz TA. 2009. Formation of the first peptide bond: the structure of EF-P bound to the 70S ribosome. *Science* 325:966–70
143. Zavialov AV, Ehrenberg M. 2003. Peptidyl-tRNA regulates the GTPase activity of translation factors. *Cell* 114:113–22
144. Spahn CM, Gomez-Lorenzo MG, Grassucci RA, Jorgensen R, Andersen GR, et al. 2004. Domain movements of elongation factor eEF2 and the eukaryotic 80S ribosome facilitate tRNA translocation. *EMBO J.* 23:1008–19
145. Sharma D, Southworth DR, Green R. 2004. EF-G-independent reactivity of a pre-translocation-state ribosome complex with the aminoacyl tRNA substrate puromycin supports an intermediate (hybrid) state of tRNA binding. *RNA* 10:102–13
146. Aitken CE, Petrov A, Puglisi JD. 2010. Single ribosome dynamics and the mechanism of translation. *Annu. Rev. Biophys.* 39:491–513
147. Frank J, Zhu J, Penczek P, Li Y, Srivastava S, et al. 1995. A model of protein synthesis based on cryo-electron microscopy of the *E. coli* ribosome. *Nature* 376:441–44
148. Tama F, Valle M, Frank J, Brooks CL 3rd. 2003. Dynamic reorganization of the functionally active ribosome explored by normal mode analysis and cryo-electron microscopy. *Proc. Natl. Acad. Sci. USA* 100:9319–23
149. Wriggers W, Agrawal RK, Drew DL, McCammon A, Frank J. 2000. Domain motions of EF-G bound to the 70S ribosome: insights from a hand-shaking between multi-resolution structures. *Biophys. J.* 79:1670–78
150. Allen GS, Zavialov A, Gursky R, Ehrenberg M, Frank J. 2005. The cryo-EM structure of a translation initiation complex from *Escherichia coli*. *Cell* 121:703–12
151. Myasnikov AG, Marzi S, Simonetti A, Giuliodori AM, Gualerzi CO, et al. 2005. Conformational transition of initiation factor 2 from the GTP- to GDP-bound state visualized on the ribosome. *Nat. Struct. Mol. Biol.* 12:1145–49
152. Klaholz BP, Myasnikov AG, Van Heel M. 2004. Visualization of release factor 3 on the ribosome during termination of protein synthesis. *Nature* 427:862–65
153. Gao H, Zhou Z, Rawat U, Huang C, Bouakaz L, et al. 2007. RF3 induces ribosomal conformational changes responsible for dissociation of class I release factors. *Cell* 129:929–41
154. Agrawal RK, Sharma MR, Kiel MC, Hirokawa G, Booth TM, et al. 2004. Visualization of ribosome-recycling factor on the *Escherichia coli* 70S ribosome: functional implications. *Proc. Natl. Acad. Sci. USA* 101:8900–5
155. Gao N, Zavialov AV, Li W, Sengupta J, Valle M, et al. 2005. Mechanism for the disassembly of the posttermination complex inferred from cryo-EM studies. *Mol. Cell* 18:663–74
156. Fu J, Kenney D, Munro JB, Lei J, Blanchard SC, Frank J. 2009. The P-site tRNA reaches the P/E position through intermediate positions. *J. Biomol. Struct. Dyn.* 26:794–95
157. Pan D, Kirillov S, Zhang CM, Hou YM, Cooperman BS. 2006. Rapid ribosomal translocation depends on the conserved 18–55 base pair in P-site transfer RNA. *Nat. Struct. Mol. Biol.* 13:354–59
158. Pan D, Kirillov SV, Cooperman BS. 2007. Kinetically competent intermediates in the translocation step of protein synthesis. *Mol. Cell* 25:519–29
159. Shoji S, Walker SE, Fredrick K. 2006. Reverse translocation of tRNA in the ribosome. *Mol. Cell* 24:931–42
160. Konevega AL, Fischer N, Semenkov YP, Stark H, Wintermeyer W, Rodnina MV. 2007. Spontaneous reverse movement of mRNA-bound tRNA through the ribosome. *Nat. Struct. Mol. Biol.* 14:318–24
161. Qin Y, Polacek N, Vesper O, Staub E, Einfeldt E, et al. 2006. The highly conserved LepA is a ribosomal elongation factor that back-translocates the ribosome. *Cell* 127:721–33
162. Scheres SH, Valle M, Grob P, Nogales E, Carazo JM. 2009. Maximum likelihood refinement of electron microscopy data with normalization errors. *J. Struct. Biol.* 166:234–40
163. Scheres SH, Gao H, Valle M, Herman GT, Eggermont PP, et al. 2007. Disentangling conformational states of macromolecules in 3D-EM through likelihood optimization. *Nat. Methods* 4:27–29

164. Zhang W, Kimmel M, Spahn CM, Penczek PA. 2008. Heterogeneity of large macromolecular complexes revealed by 3D cryo-EM variance analysis. *Structure* 16:1770–76
165. Penczek PA, Yang C, Frank J, Spahn CM. 2006. Estimation of variance in single-particle reconstruction using the bootstrap technique. *J. Struct. Biol.* 154:168–83
166. Shaikh TR, Barnard D, Meng X, Wagenknecht T. 2009. Implementation of a flash-photolysis system for time-resolved cryo-electron microscopy. *J. Struct. Biol.* 165:184–89
167. Lu Z, Shaikh TR, Barnard D, Meng X, Mohamed H, et al. 2009. Monolithic microfluidic mixing-spraying devices for time-resolved cryo-electron microscopy. *J. Struct. Biol.* 168:388–95
168. Cornish PV, Ha T. 2007. A survey of single-molecule techniques in chemical biology. *ACS Chem. Biol.* 2:53–61
169. McKinney SA, Joo C, Ha T. 2006. Analysis of single-molecule FRET trajectories using hidden Markov modeling. *Biophys. J.* 91:1941–51
170. Qin F, Auerbach A, Sachs F. 2000. A direct optimization approach to hidden Markov modeling for single channel kinetics. *Biophys. J.* 79:1915–27
171. Andrec M, Levy RM, Talaga DS. 2003. Direct determination of kinetic rates from single-molecule photon arrival trajectories using hidden Markov models. *J. Phys. Chem. A* 107:7454–64
172. Qin F, Auerbach A, Sachs F. 2000. Hidden Markov modeling for single channel kinetics with filtering and correlated noise. *Biophys. J.* 79:1928–44

Annual Review of Biochemistry

Volume 79, 2010

Contents

Indexes

Errata

An online log of corrections to *Annual Review of Biochemistry* articles may be found at http://biochem.annualreviews.org